A Scaling Investigation of Feasibility and Hover Endurance for Electric Quasi Quadrotor Configurations

by

Budhyant Venepalli
budhyant.venepalli@mavs.uta.edu

Doctoral Dissertation

Presented to the Faculty of the Graduate School of
The University of Texas at Arlington in Partial Fulfillment
of the Requirements for the Degree of

DOCTOR OF PHILOSOPHY

Department of Mechanical and Aerospace Engineering
The University of Texas at Arlington
Arlington, TX 76019

August 2020

Doctoral Dissertation Committee

Dr. D. Stefan Dancila, Associate Professor, MAE
Committee Chair

_____

Dr. Brian Dennis, Professor, MAE
Committee Member

_____

Dr. Wei-Jen Lee, Professor, EE
Committee Member

_____

Dr. Seiichi Nomura, Professor, MAE
Committee Member

_____

Dr. Dudley Smith, Professor of Practice, MAE
Committee Member

_____

Dr. Donald Wilson, Professor, MAE
Committee Member

_____

To my late father, *Ravinder Rao Venepalli*

and

my mother, *Anuradha Venepalli*

Acknowledgments

I would like to express my gratitude to my mentor and advisor, Dr. D. Stefan Dancila for his inspiring guidance and support over the course of my graduate study. He has generously offered several independent study courses which strengthened my understanding of the science of flight and made my vertical lift/rotorcraft certification possible. More importantly, I thank him for nurturing my curiosity and helping me to learn-to-learn.

I am very thankful to Mr. Mark Dreier and Dr. Dudley Smith, who have taken the time to answer numerous questions related to rotorcraft and for the motivation. I am grateful to Dr. Brian Dennis, Dr. Wei-Jen Lee, Dr. Seiichi Nomura, and Dr. Donald Wilson for serving on the Doctoral Dissertation Committee and for their guidance.

I would also like to thank my fellow graduate researchers and friends, Mr. Anirudh Srinivasan, and Mr. Soham Umbrajkar. I have greatly benefitted from many technical discussions and their companionship. I would like to extend my gratitude to all my friends for keeping my morale high and for the encouragement. I am grateful to all people who supported me financially at the beginning of my graduate studies. Many thanks to Mr. Brian Shonkwiler for his help with the Structures Lab.

I could never adequately acknowledge my parents for their continuous love, support, and sacrifice. Most importantly, I thank my sister Gopija Venepalli for her unconditional love and encouragement.

Abstract

Motivated by recent developments in distributed propulsion electric vehicles, an effort is made in the present study to numerically investigate the upper bound of hover endurance achievable by electric quasi-quadrotors at various mass scales in the range of 10^{-1} kg to 10^{4} kg total vehicle mass.

A feasible rotor propulsion pod design space is determined considering physics-based conceptual design constraints defined by blade tip Mach number and Reynolds number to ensure effective and energy-efficient generation of lift.

A conceptual level scaling optimization for two-bladed rotor quasi-quadrotors was carried out at constant blade tip speed. A momentum theory model, a blade element theory model, and a blade element momentum theory model, respectively, were used to calculate the hover endurance for an electric propulsor pod, defined as a vertically stacked configuration of a fixed pitch solid blade carbon fiber rotor, driven by a state of the art permanent magnet motor, and powered by a state of the art Li-ion battery.

Results obtained show that on the one hand individual propulsor pods which are too small cannot be optimal in hover, as the low Reynolds number has adverse effects on aerodynamics. On the other hand, pods that are too large cannot be optimal in hover as the blade mass penalty increases. It is consequently found that an optimal propulsor pod size exists, for which the hover endurance is optimal. Hence, results show that modular, endurance optimal design is achievable for larger vehicles using multiple optimal pods while preserving the optimal endurance.

Table of Contents

List of Symbols

Greek Symbols:

α	sectional angle of attack
β	specific power for motor, W/kg
ϵ	specific energy for battery, Wh/kg
ϕ	inflow angle
κ	induced power correction factor
λ	inflow ratio
μ	dynamic viscosity of air, kg/ms
θ	geometric twist
ρ	density of air, kg/m^3
σ	solidity of the rotor
τ	hover endurance, hours
Λ	blade aspect ratio
Ω	rotational speed of the rotor, rad/s

Roman Symbols:

b	number of blades
c	chord of the airfoil, m
c_{d0}	mean drag coefficient of the airfoil
g	acceleration due to gravity, m/s^2
m	quasi-quadrotor multiplicity factor
r	radial location
t	thickness of airfoil as a percentage of chord
A	area of the rotor, m^2
C_d	sectional drag coefficient
C_l	sectional lift coefficient
$C_{l\alpha}$	lift curve slope
C_P	coefficient of power
C_T	coefficient of thrust

K_A airfoil area correction factor

M mass, kg

M Mach number

P hover power, W

R radius, m

Re Reynolds number

T thrust, N

TR taper ratio

Subscripts:

B battery

EM electric motor

R rotor

T total

List of Figures

List of Tables

1. Introduction

Vertical Take-Off and Landing (VTOL) aircraft represent a category of flight vehicles which have unique flight capabilities such as runway independent operations and hover, enabling missions which are not possible with fixed wing aircraft.

For hover, VTOL vehicles rely upon thrust, which is determined by the rate of momentum change imparted upon the fluid. The rate of change in momentum is a product of the mass flow rate ($\dot{m}$) and the total change in velocity (ΔV) imparted. For a given lift, the power required to impart the rate of change in momentum is lower when a large mass flow rate is imparted a low velocity change (rotors/propellers) compared to the power required by a low mass flow rate imparted a very high velocity change (jet engine exhaust). Hence, helicopters, with low disk loading (thrust per unit area) rotors, are energy efficient in hover compared to other VTOL aircraft.

Aerospace vehicles require powerplants with a high specific power (power per unit mass) engine, using fuel with high specific energy (energy per unit mass), as weight has a strong penalty on their performance. Particularly, rotorcraft are even more demanding as their capability to hover is associated with high power requirements.

One of the reasons for the relatively late development of rotary wing aircraft compared to fixed wing aircraft was the low specific power of early piston based Internal Combustion (IC) engines powered by hydrocarbon fuels. Turboshaft engines using jet fuels with high specific energy and high energy density (energy per unit volume), developed at a later stage of technological progress are characterized by much higher specific power and have enabled the design of very large and powerful helicopters.

1.1 Conventional Powerplants

Energy generated by IC engines through the combustion of fuel-air mixture and expansion of high pressure, high-temperature combustion products following

specific thermodynamic cycles is converted into mechanical energy. From the standpoint of thermodynamics, the higher the temperature difference between the intake and the combustion products, the higher the energy available to be converted to mechanical energy, and the higher the efficiency of the system.

The heat generated in an engine is proportional to the volume of the engine and therefore is proportional to length cubed. On the other hand, the heat exchanged is a function of the surface area and therefore it is directly proportional to length squared. This means that on the one hand, larger engines are difficult to cool sufficiently and that on the other smaller engines are inefficient because of heat losses. In general, the specific power increases, and specific fuel consumption decreases for larger IC engines.

IC engines induce weight penalties when multiple engines of equivalent combined power are used instead of a single larger engine (Fig 1.1). Hence, traditionally the use of one larger engine is preferred to multiple engines having the same total combined power. Exceptions are helicopters and aircraft where two or more engines are used to increase redundancy, paying a penalty with increased weight and mechanical complexity.

For the Single Main Rotor and Tail Rotor (SMR-TR) helicopter configuration the need to use a swashplate for rotor control, a rotor hub, a transmission, a gearbox, a tail rotor, and the associated drive mechanism introduce additional mechanical complexity, weight penalty, cost, and reductions in reliability.

The SMR-TR helicopter requires a tail rotor to counter the torque generated by the main rotor and to provide yaw control. The tail rotor alone consumes about 10 to 14% of the power required in hover. Turboshaft engines which power SMR-TR helicopters operate at a very high RPM, therefore a gearbox is required to decrease it to an operating RPM which complies with the advancing blade compressibility limit and the rotor noise limit.

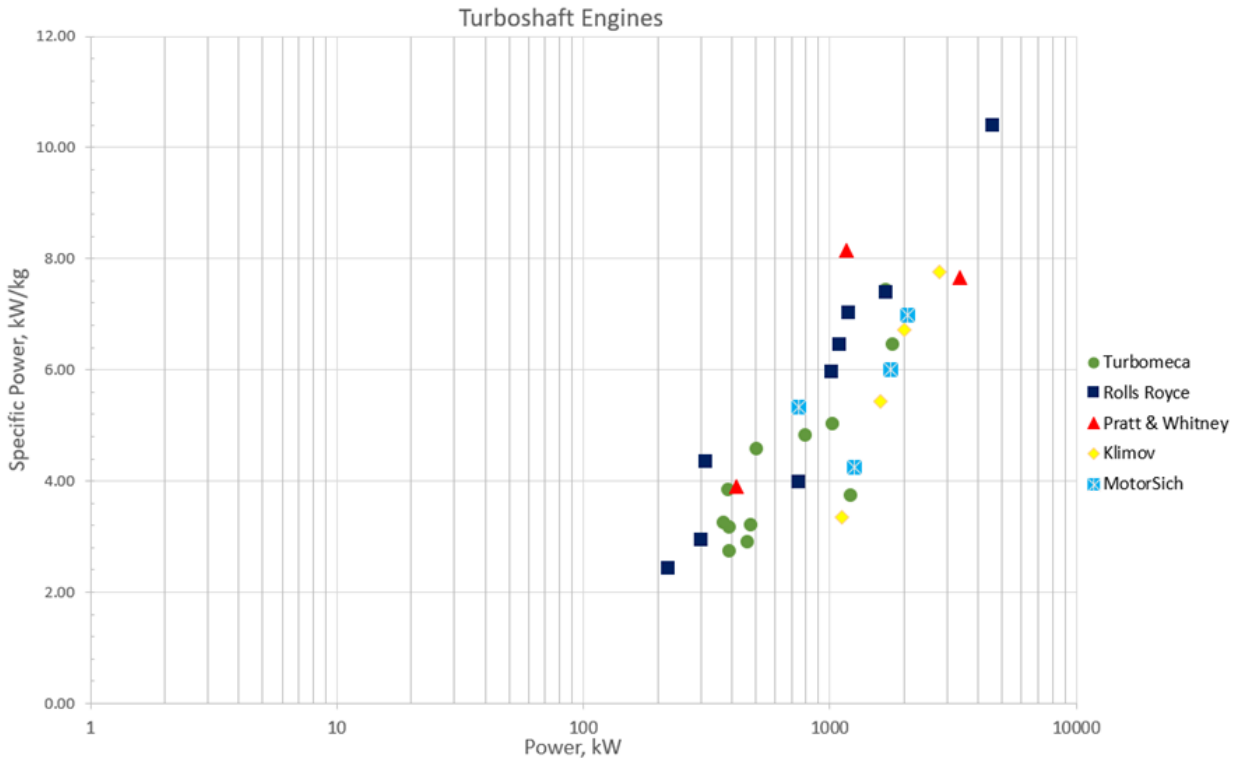

Figure 1.1: Variation of specific power vs power in turboshaft engines

The main transmission draws torque from the gearbox and drives the main rotor and the tail rotor using additional mechanism. A swashplate enables one to transfer control inputs (collective and cyclic) from a non-rotating frame to rotating rotor blades. Figure 1.2 shows major component weight contribution as a percentage of empty weight with increasing Take-Off Gross Weight (TOGW) from left to right [1].

Coaxial and tandem helicopters have two rotors, with both rotors contributing towards the thrust generation and control. Each rotor counters the torque generated by the other rotor, eliminating the requirement of a tail rotor. However, a co-axial helicopter requires a complex swashplate mechanism and a special transmission to power both rotors. Similarly, a tandem helicopter also requires a complex transmission. Even though the requirement of a tail rotor is removed, these rotorcraft introduce their own mechanical complexities and additional weight penalties.

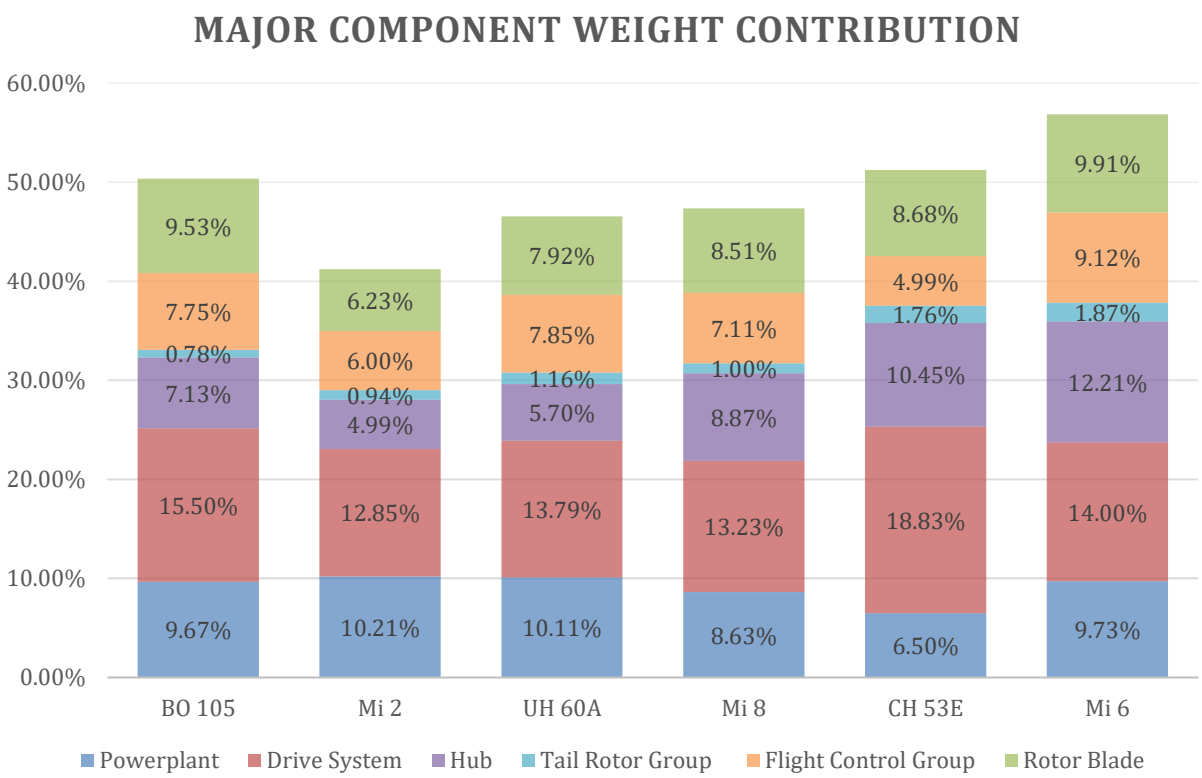

Figure 1.2: Major component weight contribution of helicopters [1]

1.2 Electric Propulsion

Recent progress in battery and electric motor technologies have motivated investigations and the development of numerous electric flight vehicles, including VTOL aircraft such as E-Volo, Joby S2, and others. By leveraging the capability of electric motors to operate efficiently over a wide range of RPM and the simplicity and convenience of Electronic Speed Control (ESC), distributed propulsion electric flight vehicles rely upon RPM control of fixed pitch propellers. Consequently, there are system level reductions in vehicle complexity, improved system reliability, and increased vehicle maneuverability.

As an example, quadrotors, deriving their lift from two pairs of two counter-rotating propellers, successfully demonstrated and implemented initially at a reduced scale, eliminated the requirement for a gearbox, a transmission, and a

swashplate mechanism typical of conventional SMR-TR helicopter configurations. An extension of the quadrotor concept, referred to in this work as the Quasi-Quadrotor (QQ), consists in a configuration characterized by the substitution of each of the four rotors by a set of identical co-rotating rotors.

1.3 Scaling Question

In the context of electric distributed propulsion VTOL, an interesting question arises regarding the effects of scaling up vehicle size upon optimal vehicle configuration, as defined by rotor blade platforms and number of rotors, and upon optimal vehicle hover endurance.

1.4 Research Objectives

The present study aims to provide an understanding of the effects of scaling on hover performance expressed by hover endurance for an electric QQ. An effort is made to investigate the maximum hover endurance achievable by an electric QQ VTOL configuration as a function of Maximum Take-Off Mass (MTOM) M_T, across several orders of magnitude, from 10^{-1} kg to 10^4 kg, considering present-day electric motor technology with a constant specific power of 6 kW/kg and Li-Ion battery with theoretical specific energy of 390 Wh/kg [2]. Physics-based conceptual design constraints based on blade tip Reynolds and Mach numbers were established to ensure the aerodynamic efficiency for electric QQ VTOL scaling.

2. Literature Survey

Prior to recent developments in battery and electric motor technology, electric propulsion in aviation was only limited to applications such as High-Altitude Long Endurance (HALE) vehicles and small-scale Unmanned Aerial Vehicles (UAV). However, with the recent interest in the application of the matured electric propulsion technology towards urban air mobility, electric VTOL vehicles received significant attention. Literature includes a survey of propulsion technologies available [2,3], modeling/sizing of electric propulsion applicable to UAV's [4-12], and comparative studies of mission specific conceptual electric VTOL design to enable urban air mobility [13-21].

Electric motors do not incur significant weight penalty in substituting one large motor by smaller motors, thereby effectively enabling distributed propulsion. Ongoing research interest is devoted to investigating the feasibility and effects upon VTOL performance of scaling up electric QQ VTOL [22]. One such effort, Project LIFT! [23,24] is a scalable, modular, all electric multirotor platform, developed and tested by the Boeing company to fill in the need for VTOL vehicles which can lift high payloads and operate at a short range. Hover endurance of project LIFT! was tested at various gross weights (up to 500 lbs.), carrying different payload weights.

Winslow *et.al.,* [25] designed, optimized and tested a Micro Aerial Vehicle (MAV) scale quadrotor with total mass less than 50 g and it was reported that the longest continuous hover endurance measured for their design was 31minutes, which is almost double the hover endurance of any existing MAV- scale quadrotors. Due to the low Reynolds number at such a small scale, a high solidity rotor with 6.1% cambered shell was found to be optimum.

Gatti, Giulietti, and Turci [26] presented an analytical battery optimization framework for maximum hover endurance for an existing multi-rotor platform. Peukert's equation [27] was applied to estimate the energy available in the battery considering the battery capacity and the discharge rate. The power required to hover is calculated using momentum theory with a figure of merit correction, measured

from experiments. The hover endurance is calculated by varying the weight of the battery and the battery ratio for maximum endurance is determined. However, the study neither provides the upper bound of performance nor does it address the aspect of distributed propulsion.

Reference [23] emphasizes the fact that there is no required power penalty when dividing one large rotor into multiple smaller rotors of equivalent total area at a constant disk loading, thereby allowing modular design. However, it was reported that the small rotor diameter of individual disks resulted in a reduction in aerodynamic efficiency caused by low Reynolds number aerodynamic effects and interactions between the rotors.

Reference [28] summarizes the literature on the effects of Reynolds number on airfoil maximum sectional lift-to-drag ratio and provides results of a computational study, not only on thick conventional airfoils but also on thin cambered shells, between Reynolds numbers of 10^4 and 10^5. Above the Reynolds number of 10^5, conventional airfoils are known to offer high maximum sectional lift-to-drag ratios compared to thin cambered shells. It was shown that below a Reynolds number of 10^5, maximum sectional lift-to-drag ratio of conventional airfoils decreased drastically when compared to cambered shells. Hence, in this study, we choose to constrain operating conditions to blade tip Reynolds numbers higher than 10^5.

Gur and Rosen [5] presented a new method of designing an optimal propeller of an ultra-light aircraft based on a multidisciplinary design optimization approach, considering different design goals to maximize endurance in loiter and maximum airspeed. Three numerical optimization schemes, namely a simple genetic algorithm, Nelder-Mead's simplex method, and the steepest-descent method were used consecutively in the study to find the optimum design. Blade element momentum theory was used to calculate the aerodynamic forces and power required.

Beals [11] performed a design optimization study of a multirotor with a nine-inch diameter rotor to minimize the total power required to hover at standard sea-level conditions and of a larger rotor at an altitude of 4000ft. Blade element

momentum theory was used to calculate the power required to hover. Rotor blade chord distribution, twist distribution, and the RPM of the rotor were varied by holding the rotor blade radius to be constant. A hybrid optimization scheme consisting of a non-gradient-based genetic algorithm was used to initially identify the region of the global minimum followed by a gradient-based sequential quadratic programming to refine the solution. Although the approach resulted in a 29% decrease in power required to hover at sea level conditions compared to the baseline configuration, the study did not address the aspects of distributed propulsion and the effects of varying rotor blade radius.

A scalability study for an unconventional Quadrotor Biplane Tailsitter (QBiT) using a generalized design and analysis tool, Hybrid Design and Rotorcraft Analysis (HYDRA) was performed by Govindarajan, Sridharan, and Chopra [29]. Unlike conventional statistical weight estimation methods, physics-based iterative sizing/weight estimation models [30] for rotor and support structure were used.

A comprehensive, conceptual level study to understand the effects of scaling on the hover endurance of an electric distributed multirotor VTOL configuration subjected to Mach number and Reynolds number constraints was not found in the literature.

3. Approach and Methodology

The total number of rotors in a QQ VTOL design is defined by the multiplicity factor, m. For m=1, the QQ VTOL is a quadrotor, for m=2, it is an octarotor, and so on. As all the rotors in QQ are assumed to be identical in size and noninteracting, this endurance study becomes equivalent to the investigation of the endurance of a single propulsor.

Considering that each fixed pitch rotor is driven by a motor and powered by a Li-ion battery, a vertically stacked configuration allows for effective cooling, and reduction in the support structure and wiring mass. Such a configuration is referred to in this study as a unit electric propulsor pod.

The absolute upper bound of endurance is estimated for a vehicle by disregarding the payload and support structure mass. It is further considered that the total vehicle mass is equally distributed between the identical propulsors consequently, the MTOM of a QQ becomes equal to the sum of battery mass M_B, motor mass M_{EM}, and rotor mass M_R.

$$M_T = M_B + M_{EM} + M_R \quad (1)$$

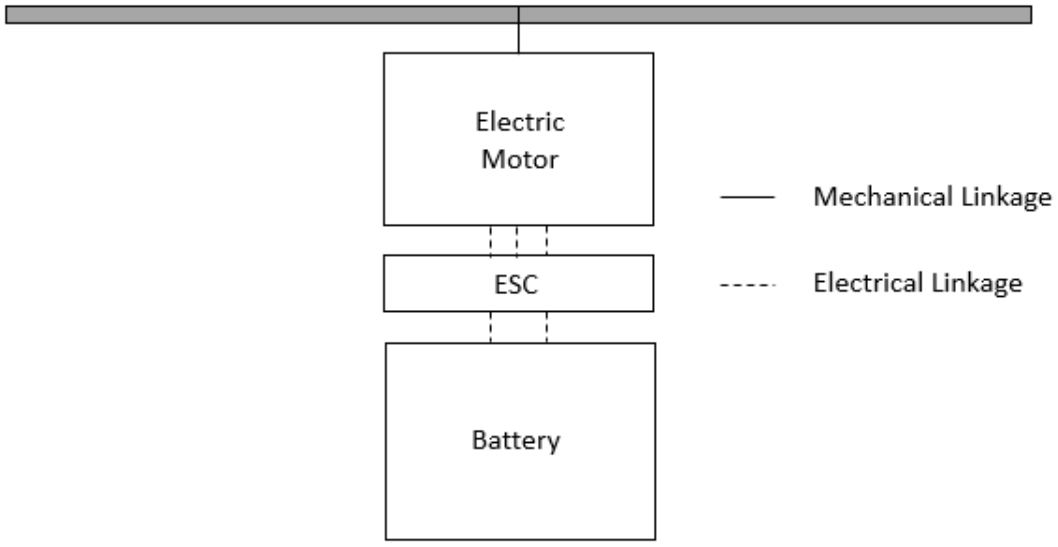

Figure 3.1: Electric propulsor pod

3.1 Mass Estimation

3.1.1 Battery Mass

Lithium is favored as the anode material for rechargeable batteries due to its small atomic size, lightweight with an equivalent mass of 6.941 g/mole and high electro-positivity which is typical of alkali metals with a standard electrode potential of -3.04 V. Lithium-Ion (Li-Ion), Lithium Sulphur (Li-S) and Lithium-air are some of the battery chemistries for which lithium is used as anode material. Table 3.1 presents theoretical specific energies for three kinds of Li based battery technologies [2].

Table 3.1: Theoretical specific energy of Li based battery technologies [2]

Battery Technology	ϵ **(Wh/kg)**
Li-Ion	390
Li-S	2570
Li-Air	3500

Li-Ion batteries have been used on electric aircraft like Solar Impulse I, Joby S2, Lange Antares sailplane and electric rotorcraft like Chretien helicopter, Sikorsky Firefly, Volta, modified R22 developed by Tier1 engineering and others. Commercially available Li-S batteries have relatively high specific energy but can only be discharged slowly, therefore they are preferred on fixed wing HALE platforms like Airbus Zephyr and Centurion where power demands are low. Lithium-air batteries are not commercially available currently and are believed to have a technology readiness level (TRL) of 4. Out of all the Lithium-based rechargeable battery chemistries available, Li-ion chemistry is considered for the present study due to its technological maturity.

The smallest constitutive unit of a battery is an electrochemical cell, with the voltage corresponding to the chemistry used, called the nominal voltage and the cell capacity defined by its volume. When such cells are connected in series their cell voltage adds up, but the capacity remains the same. On the other hand, when cells are connected in parallel cell voltage remains the same and capacity adds up.

Table 3.2 shown below provides performance metrics of ultra-high energy Lithium-Nickel Manganese Cobalt Oxide cells, developed by Kokam batteries [31]. They are designed to offer a high heat dissipation rate, low internal resistance, and high efficiency. Even though these cells have high specific energy, battery packs made using these cells have a lower specific energy.

Table 3.2: Kokam Li-ion cell performance metrics [31]

Model	**Capacity (Ah)**	**Width (mm)**	**Length (mm)**	**Thickness (mm)**	**Internal resistance (mΩ)**	**Mass (kg)**	**C rate factor: max.**	**C rate factor: peak**	**Specific energy (Wh/kg)**
1	12	80	181	6.3	2.8	0.17	2	4	257
2	27	95	272	7.6	1.6	0.38	2	4	260

Out of the total energy available in a battery, only about 80% can be utilized as the battery losses its reusability when all its available energy is drawn out. The rate of discharge also determines the amount of energy available in a battery, among other factors. Modeling of these phenomena involves all the performance metrics mentioned in Table 3.2 and a battery model based on equivalent circuits at the minimum.

For a conceptual level study assuming a hypothetical battery providing its theoretical specific energy, it is not possible to develop and use the specific characteristics involved in estimating the energy stored in the cell. Therefore, in this

study, a rubber battery model is considered, and for a given power P, endurance τ and theoretical specific energy ϵ=390 Wh/kg, the mass of the battery can be determined by

$$M_B = \frac{P\,\tau}{\epsilon} \tag{2}$$

3.1.2 Electric Motor Mass

High power electric motors based on rare earth permanent magnets are developed for specific high-efficiency applications such as electric vehicles. However, the design of motors intended for land-based vehicles employs lower constraints such as specific power, power density, and cooling needs, compared to aerospace applications.

Siemens manufactures an electric motor with a specific power of 5.2 kW/kg for the Extra 330LE electric plane. At a comparable power, the motors available for industrial applications and electric vehicles only offer approximately 1 kW/kg and 2 kW/kg, respectively [32].

Considering proportional variation between the power and mass of the motor, with a constant specific power β of 6 kW/kg as suggested by Walter [33], the mass of electric motor including ESC can be determined for the present investigation by

$$M_{EM} = \frac{P}{\beta} \tag{3}$$

3.1.3 Rotor Mass

Results of prior investigations of rotor blade weight scaling trends published in the literature for specific combinations of rotor blade materials and structural concept show a power-law dependence on the scaling parameter, R – the rotor blade radius, with an exponent in the range between 2.3 [34] to 2.89 [35]. It is important to note that with a change in scale, not only the cross-section but also the material demands of the rotor blade change.

Given the conceptual and analytical nature of this study, we use a structural concept based on solid carbon fiber blades as a conservative first-order approximation. The mass of the rotor is directly proportional to the number of blades

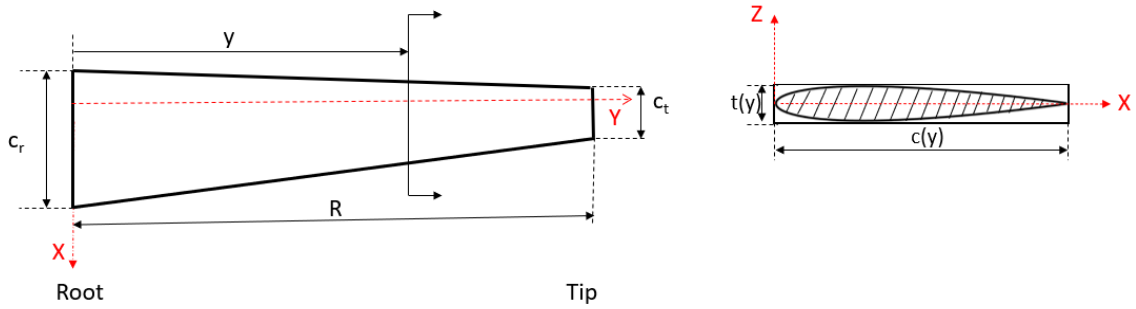

Figure 3.2: Geometric description of the tapered propulsor blade

b, the volume of each blade and the density of blade material (ρ_b =1600 kg/m^3) used. Considering rectangular, constant chord solid carbon fiber blades, with a factor K_A accounting for airfoil cross-sectional area $A_{Airfoil}$, as shown in the figure above, the mass of a single blade can be written as

$$M_b = \rho_b \, A_{Airfoil} \, R \tag{4}$$

$$M_b \cong \rho_b \, (K_A t \, c^2) R \tag{5}$$

Expressing the chord c of the blade in terms of the aspect ratio Λ, and rewriting Eqn. 5, we obtain the mass for the blade and the rotor as

$$M_b \cong \frac{\rho_b \, K_A t}{\Lambda^2} \, R^3 \tag{6}$$

$$M_R \cong b \, M_b \cong \frac{\rho_b \, K_A t}{\Lambda^2} \, b \, R^3 \tag{7}$$

Here, K_A is 0.60 as suggested by Drela, and the thickness percentage of the airfoil t, is taken as 12 percent.

Considering linearly tapered carbon fiber blades as shown in Fig. 3.2, with a root cord c_r and a tip chord c_t, we define propulsor blade taper ratio TR, as the ratio of the tip chord to the root chord. For linearly tapered blades, the mass of a single blade Eqn. 5 translates to

$$M_b \cong \int_0^R \rho_b \, K_A t \, c(y)^2 \, dy \tag{8}$$

$$M_b \cong \rho_b \, K_A t \int_0^R (c_r - \frac{c_r - c_t}{R} y)^2 \, dy \tag{9}$$

Equation 9 reduces to

$$M_b \cong \rho_b K_A t \left(c_r{}^2 R + (c_r - c_t)^2 \frac{R}{3} - c_r(c_r - c_t)R\right) \quad (10)$$

Rewriting Eqn. 10 in terms of the taper ratio, $TR = \frac{c_t}{c_r}$ and simplifying we have

$$M_b \cong \frac{1}{3} \rho_b K_A t \, c_r{}^2 (1 + TR + TR^2) R \quad (11)$$

Expressing the root chord c_r in terms of the aspect ratio Λ, and simplifying Eqn. 11, we have

$$M_b \cong \frac{4}{3} \rho_b K_A t \frac{1+TR+TR^2}{1+2TR+TR^2} \frac{R^3}{\Lambda^2} \quad (12)$$

Where aspect ratio for tapered blades is

$$\Lambda = \frac{R^2}{S} = \frac{R^2}{R\, c_t + \frac{1}{2}(c_r - c_t)R} = \frac{2R}{c_r(1+TR)} \quad (13)$$

Substituting Eqn. 12 in 7, we obtain the mass of the rotor as

$$M_R \cong \frac{4}{3} b \, \rho_b K_A t \frac{1+TR+TR^2}{1+2TR+TR^2} \frac{R^3}{\Lambda^2} \quad (14)$$

3.2 Endurance Calculation

Unlike conventional aircraft powered by fuel, the weight of the electric VTOL vehicles does not reduce during flight, given that no part of the vehicle is jettisoned, thereby placing electric VTOL vehicles at a disadvantage. However, this makes the estimation of endurance simpler, using Eqns. 1, 2, 3 and 14, we have

$$\tau_{QQ} = \frac{\epsilon}{P_{QQ}} [M_T - 4m M_R] - \frac{\epsilon}{\beta} \quad (15)$$

3.3 Power Calculation

The present study considers four models with increasing order of refinement, for the calculation of the power required in hover, which is based on

- Model 1: Momentum theory, with an induced power correction factor, κ
- Model 2: Blade element theory, with mean airfoil drag coefficient, c_{d0}
- Model 3: Blade element theory, with three-term drag polar and linear twist, and
- Model 4: Blade element momentum theory, with linear twist and taper

3.3.1 Model 1

To analytically investigate the upper bound of hover endurance, we consider momentum theory [36] for the prediction of the power required to hover, with zero rotor mass. Therefore, for an ideal rotor with rotor disk area A, providing a given thrust T, we can determine the power required to hover P_{QQ}, by

$$P_{QQ} = 4\,m \frac{\kappa T^{3/2}}{\sqrt{2\,\rho_\infty\,A}} \tag{16}$$

Here, we consider the induced power correction factor κ, to be 1.15, and the density of air ρ_∞, at standard atmospheric conditions is 1.225 kg/m^3. We can write Eqn. 16 as

$$P_{QQ} = 4\,m \frac{\kappa \left(\frac{M_T\,g}{4\,m}\right)^{3/2}}{\sqrt{2\,\rho_\infty\,A}} \tag{17}$$

3.3.2 Model 2

The power required by a real rotor to hover is equal to the sum of the induced power and the profile power. Equation 18 accounts for the induced power provided by Model 1 and the profile power based on the mean sectional drag coefficient of the airfoil [36]. The total power required by QQ is obtained by

$$P_{QQ} = 4m\,(P_i + P_o) \tag{18}$$

$$P_{QQ} = 4\,m \left(\frac{\kappa \left(\frac{M_T\,g}{4\,m}\right)^{3/2}}{\sqrt{2\,\rho_\infty A}} + \rho_\infty\,A\,(\Omega R)^3 \frac{\sigma\,c_{d0}}{8} \right) \tag{19}$$

Assuming that the tip speed ΩR remains constant throughout, we express tip speed in terms of the tip Mach number $M_{tip,}$ and the speed of sound a_∞. For rectangular blades, solidity σ can be expressed in terms of the number of blades and the aspect

ratio of the blades. The sectional mean drag coefficient for twelve percent thick airfoils is estimated to be 0.01. Therefore, using Eqn. 19 the power required by QQ is given by

$$P_{QQ} = 4\,m\left(\frac{\kappa\left(\frac{M_T\,g}{4\,m}\right)^{3/2}}{\sqrt{2\,\rho_\infty\,A}} + \rho_\infty\left(M_{tip}\,a_\infty\right)^3\frac{b\,c_{d0}\,R^2}{8\,\Lambda}\right) \tag{20}$$

3.3.3 Model 3

The coefficient of power C_P and the coefficient of thrust C_T [36] for a real rotor with rectangular blades, considering no root cutout and tip losses, with inflow angle ϕ, normalized radius r, the sectional lift coefficient C_l, and the sectional drag coefficient C_d, considering small angle assumptions, we have

$$C_P = \frac{1}{2}\sigma\int_0^1(\phi\,C_l + C_d)\,r^3dr \tag{21}$$

$$C_T = \frac{1}{2}\sigma\int_0^1 C_l\,r^2dr \tag{22}$$

Equations above were solved numerically using the rectangular rule considering N radial stations along the blade. The elemental thrust and the inflow are considered to be constant over the blade element. Therefore Eqns. 21 and 22, can be written as

$$C_P = \sum_{n=1}^{N}\frac{\sigma}{2}(\phi\,C_l + C_d)r^3dr \tag{23}$$

$$C_T = \sum_{n=1}^{N}\frac{\sigma}{2}C_l\,r^2dr \tag{24}$$

For rectangular blades, solidity can be expressed in terms of the number of blades and the aspect ratio of the blades. Considering linear geometric twist θ and uniform inflow λ defined in terms of the coefficient of thrust C_T, we have

$$\theta(r) = \theta_0 + r\theta_1 \tag{25}$$

$$\lambda(r) \cong \lambda \cong \sqrt{\frac{C_T}{2}} \cong \sqrt{\frac{M_T\,g}{8\,m\,\rho_\infty A\left(M_{tip}\,a_\infty\right)^2}} \tag{26}$$

The sectional lift and drag characteristics of an airfoil are a function of the sectional angle of attack α, the Reynolds number and the Mach number. However, for this study a linear approximation for lift coefficient with the lift curve slope $C_{l\alpha}$ equal

to 5.7 and three-term drag polar approximation for sectional drag coefficient [37] defined by Eqn. 28 are considered.

$$C_l = 5.7\,\alpha \tag{27}$$

$$C_d = 0.0087 - 0.0216\,\alpha + 0.4\,\alpha^2 \tag{28}$$

$$\alpha(r) = \theta(r) - \phi(r) = \theta(r) - \frac{\lambda(r)}{r} \tag{29}$$

For a given total mass, number of blades, multiplicity, blade aspect ratio, and blade radius, θ_1 is varied while adjusting θ_0 to produce the required thrust, using a modified bisection method [36]. The geometric twist distribution which provides a minimum coefficient of power is selected and its respective power required to hover is calculated, followed by mass calculation for the rotor, motor, and the battery. If the mass of the battery is greater than zero, endurance is calculated using Eqn. 15. The blade radius and the aspect ratio are then varied using a numerical optimization

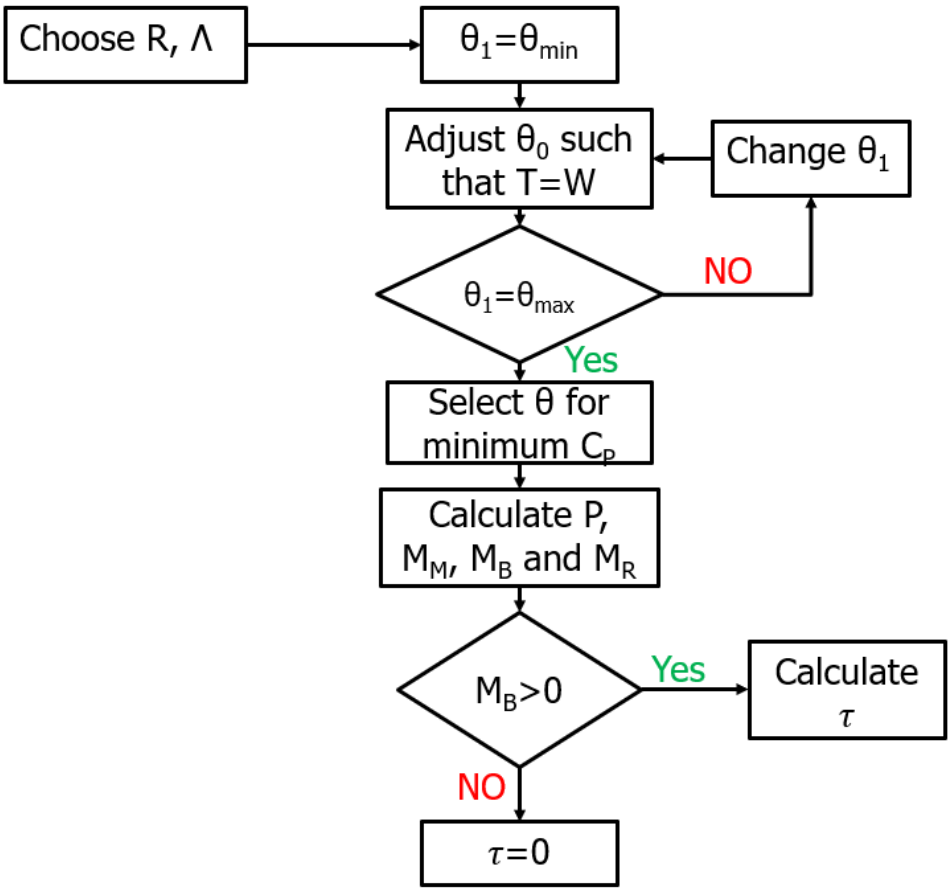

Figure 3.3: Hover endurance calculation algorithm

scheme described in section 3.5. Figure 3.3 shows a detailed description of the approach used. The total power required to hover and the thrust generated, are calculated from the coefficient of power and the coefficient of thrust using equations below, respectively.

$$P_{QQ} = 4\,m\,C_P\,\rho_\infty A\left(M_{tip}\,a_\infty\right)^3 \tag{30}$$

$$T_{QQ} = 4\,m\,C_T\,\rho_\infty A\left(M_{tip}\,a_\infty\right)^2 \tag{31}$$

3.3.3 Model 4

The blade element momentum theory [36] allows the calculation of the radial inflow variations of a hovering rotor defined by Eqn. 32, by combining both blade element and momentum theory approaches on an annulus by annulus basis. Following the approach mentioned in Model 3, the power required to hover can be calculated considering non-uniform inflow.

$$\lambda(r) = \frac{\sigma\,C_{l_\alpha}}{16}\left(\sqrt{1+\frac{32}{\sigma\,C_{l_\alpha}}\,\theta\,r}-1\right) \tag{32}$$

Prandtl [36] suggested a correction factor F, to account for the loss of lift near blade tips resulting from induced effects associated with a finite number of blades. The radial inflow equation and the coefficient of thrust generated needs to be modified to incorporate the tip losses, we have

$$\lambda(r) = \frac{\sigma\,C_{l_\alpha}}{16\,F}\left(\sqrt{1+\frac{32\,F}{\sigma\,C_{l_\alpha}}\,\theta\,r}-1\right) \tag{33}$$

$$C_T = 4\int_0^1 F\,\lambda^2 r\,dr \tag{34}$$

Where F is defined by the equation

$$F(r) = \left(\frac{2}{\pi}\right)\cos^{-1}\left(e^{-f}\right) \tag{35}$$

$$f = \frac{b}{2}\left(\frac{1-r}{r\,\phi}\right) \tag{36}$$

Equations 33, 35, and 36, were written as a single equation and solved iteratively using the interval halving technique as described by Dreier [38]. The technique finds the root of the combined equation by initially solving the equation for

F=0, F=0.5 and F=1, consequently narrowing the region where a root exists at each radial station.

For linearly tapered blades, the chord and the blade local solidity varies along the propulsor blade radius as described by Eqn. 37 and 38, respectively.

$$c(r) = c_r - c_r(1 - TR)r \tag{37}$$

$$\sigma(r) = \frac{b\, c(r)}{\pi\, R} \tag{38}$$

Where blade root chord c_r, is defined using Eqn. 13 as

$$c_r = \frac{2\, R}{\Lambda\,(1+TR)} \tag{39}$$

3.4 Conceptual Design Constraints

The feasible design space is established by considering two important aerodynamic parameters, the Reynolds number Re, and the Mach number M, to ensure the aerodynamic efficiency of the rotor. A blade tip Mach number M_{tip}, not greater than 0.3 is chosen to avoid compressibility effects and a blade tip Reynolds number Re_{tip}, not lower than 10^5 is chosen.

The blade tip Mach number can be expressed in terms of the tip speed and the speed of sound as

$$M_{tip} = \frac{\Omega\, R}{a_\infty} \tag{40}$$

Therefore, Eqn. 40 can be written as

$$\Omega^{max} \leq \frac{M_{tip}^{max} a_\infty}{R} \tag{41}$$

Similarly, the blade tip Reynolds number can be expressed in terms of the dynamic viscosity of air μ=1.789 x 10^{-5} kg/ms, the density of air, the tip speed, and the tip chord as

$$Re_{tip} = \frac{\rho_\infty\, (\Omega R)\, c_{tip}}{\mu} \tag{42}$$

Therefore, Eqn. 42 can be written as

$$\Omega^{min} \geq \left(\frac{\mathrm{Re}_{tip}^{min}\,\mu\,\Lambda}{\rho_\infty}\right)\ \frac{1}{R^2} \tag{43}$$

Disk loading can be expressed in terms of the thrust coefficient, the blade tip speed, and the area of the disk. Therefore, for a given disk loading, we have:

$$D_L = \frac{T}{A} = \frac{\rho_\infty\,\pi\,R^2(\Omega\,R)^2 C_T}{\pi\,R^2} = \rho_{air}\,(\Omega\,R)^2 C_T \tag{44}$$

Rewriting Eqn. 46 in terms of the blade aspect ratio, blade loading and the number of blades, we have

$$\Omega = \frac{1}{R}\sqrt{\frac{D_L}{\rho_\infty\,{C_T}/{\sigma}\,\frac{b}{\pi\,\Lambda}}} = \frac{1}{R}\sqrt{\frac{\pi\,D_L\,\Lambda}{\rho_\infty\,b\,{C_T}/{\sigma}}} \tag{45}$$

3.5. Sequential Quadratic Programing

Sequential Quadratic Programming (SQP) [39] is a gradient based optimization technique where the search direction is found by solving a subproblem with a quadratic objective function subjected to linear constraints. The objective function is modified using Lagrange multipliers and an exterior penalty function so that the resulting one-dimensional search direction is unconstrained.

An approximation is made of the Hessian of the Lagrange function using a quasi-Newton updating method at each iteration [40]. Then this information is used to generate a quadratic approximation to the augmented objective function and a linear approximation to the constraints.

Considering a general statement of the problem as below

Minimize: $F(\mathbf{X})$

Subjected to: $g_j(\mathbf{X}) \leq 0 \qquad j = 1,m$

$h_k(\mathbf{X}) = 0 \qquad k = 1,l$

$X_i^l \leq X_i \leq X_i^u \qquad i = 1,n$

The direction-finding problem becomes

Minimize: $Q(\mathbf{S}) = F(\mathbf{X}) + \nabla\mathbf{F}(\mathbf{X})^T\mathbf{S} + \frac{1}{2}\mathbf{S}^T\mathbf{B}\mathbf{S}$

Subjected to: $\nabla \mathbf{g}_j(\mathbf{X})^T \mathbf{S} + \delta_j \mathbf{g}_j(\mathbf{X}) \leq 0 \qquad j = 1,m$

$$\nabla \mathbf{h}_k(\mathbf{X})^T \mathbf{S} + \bar{\delta} \mathbf{h}_k(\mathbf{X}) = 0 \qquad k = 1,l$$

Where **S** is the iteration and **B** is a positive definite matrix which is updated over subsequent iterations to approach the Hessian of the Lagrangian. In addition to it, $\bar{\delta}$ and δ_j, are scalar parameters dependent on the constraints, therefore, they are problem specific. A detailed description of the approach is described by Vanderplaats [39].

For this study, SQP is implemented within MATLAB® and the code is parallelized to run multiple cases simultaneously. Equation 15 was modified to a new function and is minimized subject to constraints described in section 3.4, to obtain a configuration for which the hover endurance is maximum.

Minimize: $$F(\mathbf{X}) = \frac{\epsilon}{\beta} - \frac{\epsilon}{P_{QQ}}[M_T - 4mM_R]$$

Subjected to: $$Re_{tip}(\mathbf{X}) \geq 10^5$$

$$M_{tip}(\mathbf{X}) = 0.3$$

Where the variables are the blade radius and the blade aspect ratio

$$\mathbf{X} = \begin{bmatrix} R \\ \Lambda \end{bmatrix}$$

Limits for the blade aspect ratio and twist rate are

$\Lambda \in [5, 20]$

$\theta_1 \in [-50, 0]$ deg/r

4. Results and Discussion

4.1 Feasible Design Space

Making use of the conceptual physics-based design constraints defined by the Eqns. 41, 43, and 45, the feasible design space is established for the design and scaling of electric QQ. To remain within the defined space, low disk loading values must be chosen.

Figure 4.1 shows that for the disk loading chosen, there exists a minimum value of radius below which the Reynolds number constraint is violated. Although a range of Ω operable as highlighted in Fig. 4.1 exits, as tip speed is considered to be constant, the blade tip Mach number, defined by Eqn. 40 is equal to 0.3.

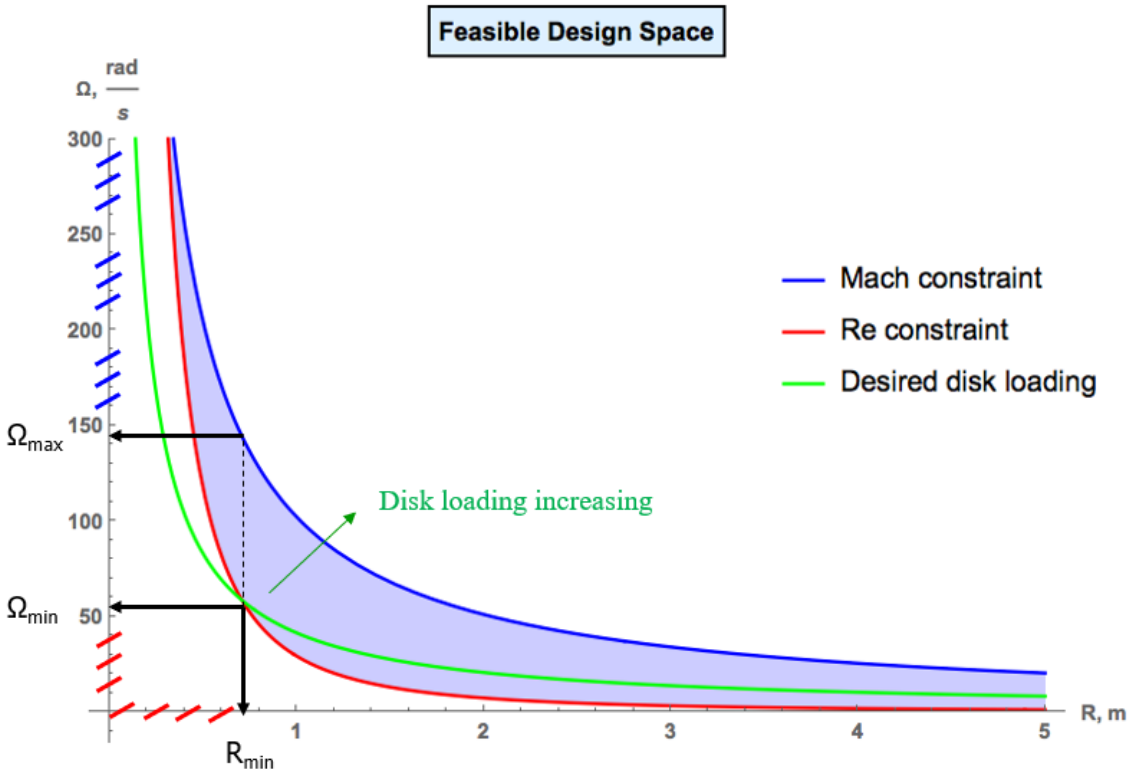

Figure 4.1: Example of feasible design space describing design constraints

4.2 Absolute Upper Bound of Hover Endurance

An overly optimistic estimation is achieved by neglecting the rotor mass and considering Model 1 for the hover power estimation. Even though such considerations result in unrealistic values, they serve as an absolute upper bound of the endurance achievable by a QQ for the given technology. Figures 4.2 and 4.3 provide the absolute upper bound of QQ with M_T of 10^{-1} and 10^4kg, respectively. Extremely high values of hover endurance are obtained in the case of vehicles with low M_T. We notice in Fig. 4.3, that for very small rotor radii, the mass of the motor required becomes equal to or exceeds MTOM due to high power demands and therefore no room for the battery is left, resulting in zero endurance.

The power calculated by Model 1 is inversely varying with the individual pod rotor radius, i.e., the hover power required for a given MTOM decreases with the increase of the radius. In addition to that, the endurance defined by Eqn. 15 is inversely varying with power. Therefore, for a given total weight and m, a direct relationship exists between the propulsor radius and the absolute endurance. Additionally, for a given value of rotor radius, increasing the number of rotors results in higher values of the endurance.

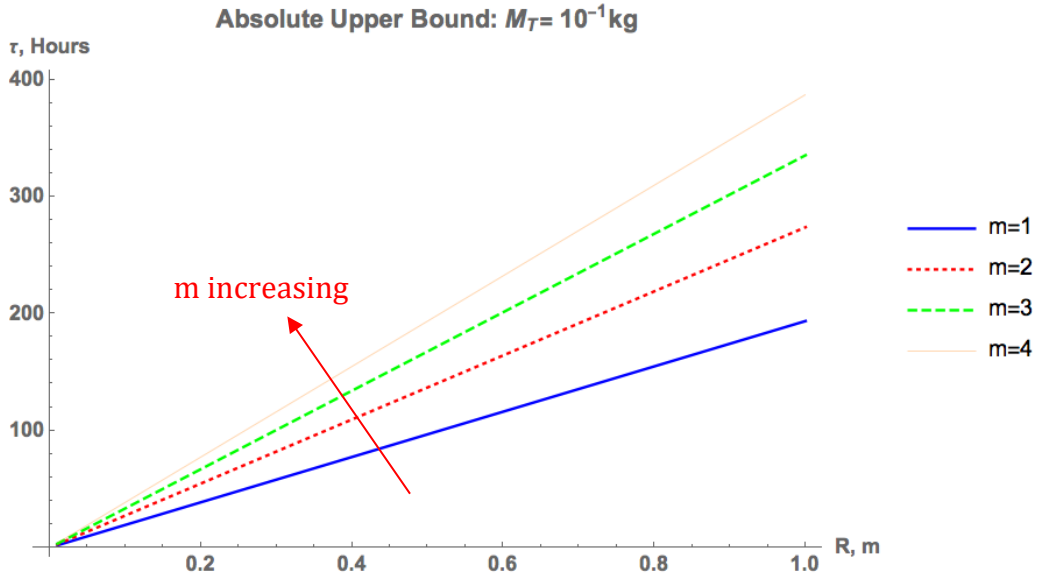

Figure 4.2: Upper bound of hover endurance achievable by QQ for $M_T = 10^{-1}$kg

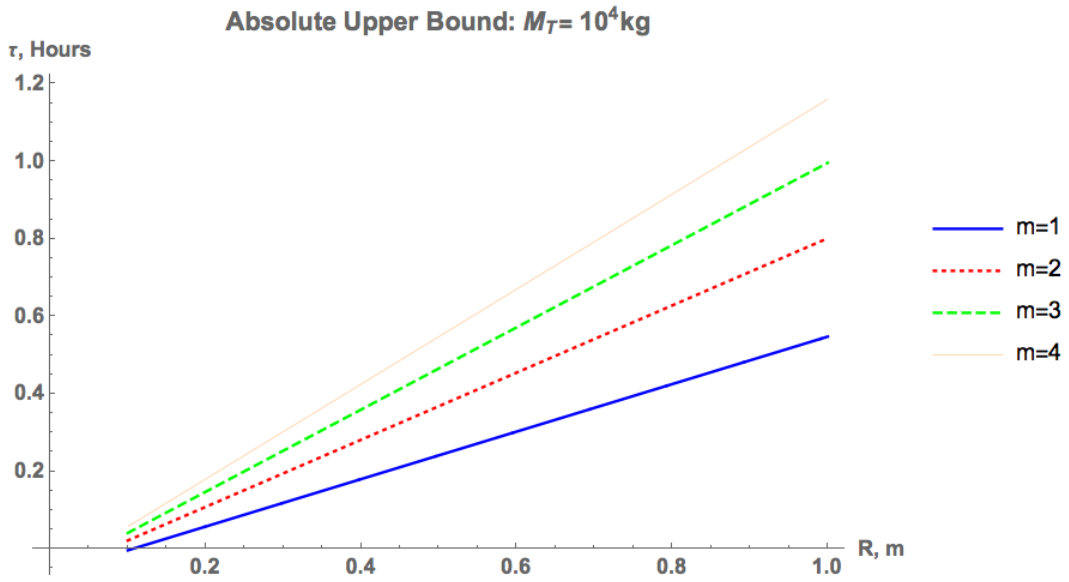

Figure 4.3: Upper bound of hover endurance achievable by QQ for $M_T = 10^4$kg

From Model 1, it is observed that at an equivalent disk loading, the endurance remains constant. This is a consequence of disregarding rotor mass and power prediction using momentum theory.

4.3 Constrained Optimization

4.3.1 Model 2

The hover endurance of an electric QQ defined by Eqn. 15 and the power estimation Model 2, depends on five parameters:

1. Total vehicle mass, M_T
2. Multiplicity factor of quasi-quadrotor, m
3. Number of blades of rotor, b
4. Aspect ratio of the blades, Λ and
5. Radius of the individual rotor, R

The Mach number constraint is enforced by considering that the tip Mach number is equal to 0.3 and the Reynolds number constraint is implemented by requiring the tip Reynolds number to be greater than 10^5. Consequently, for the given blade aspect ratio there exists a rotor radius below which Eqn. 43 is violated.

Limiting the scaling investigation to two bladed rotors with the blade aspect ratio varying from 5 to 20, optimization is carried out across several orders of magnitude of M_T by varying individual pod radius and multiplicity factor.

Quasi-quadrotor with $M_T = 10^{-1}$kg: For a quadrotor, results for unconstrained and constrained study across aspect ratios of 5, 10, 15, and 20 are shown in Figs. 4.4 and 4.5, respectively.

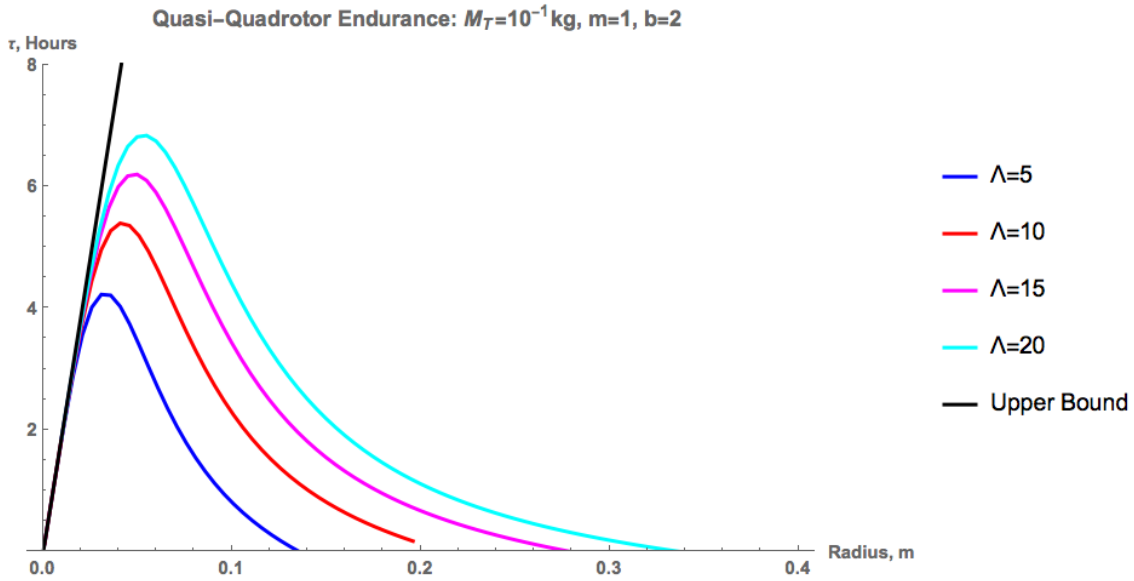

Figure 4.4: Unconstrained hover endurance from Model 2 for $M_T = 10^{-1}$kg

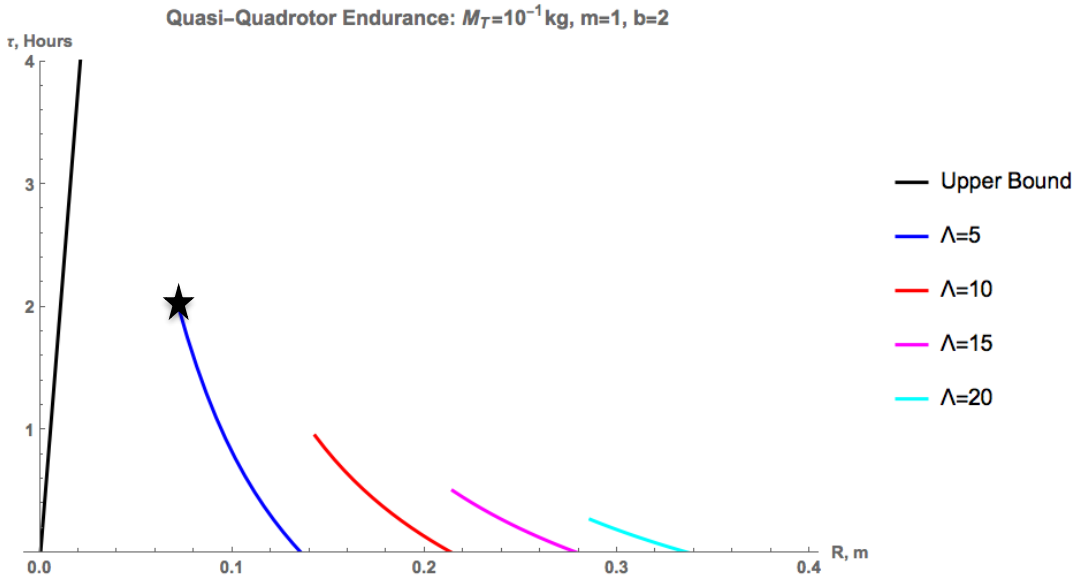

Figure 4.5: Constrained hover endurance from Model 2 for $M_T = 10^{-1}$kg

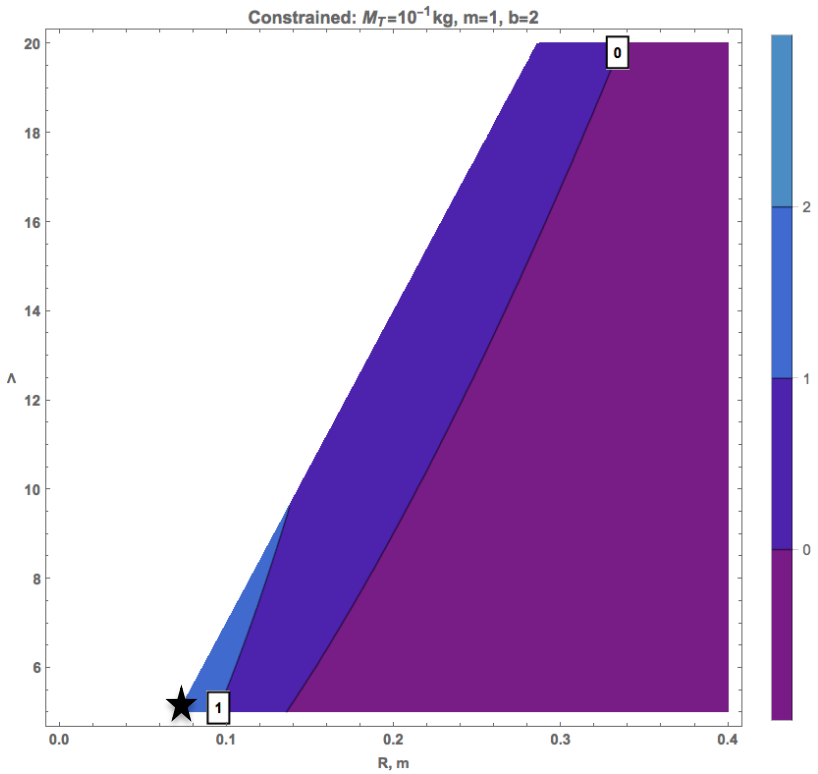

Figure 4.6: Hover endurance from Model 2 for $M_T = 10^{-1}$kg, m=1, b=2

Although unconstrained results show an increase in the endurance with an increase in the blade aspect ratio, from constrained optimization it is known due to the low tip Reynolds number, the endurance is decreased with an increase in the blade aspect ratio.

Dependence of endurance on aspect ratio is summarized in Fig. 4.6. The maximum value of endurance is obtained at the lower limit of the blade aspect ratio. Additionally, a further increase in m values had adverse effects on the endurance, suggesting that a quadrotor at the lower limit of the considered aspect ratio resulted in the maximum endurance of 2.03 hours.

Quasi-quadrotor with M_T = 1kg: Repeating the constrained study at one-kilogram mass resulted in a contour plot as illustrated in Figs. 4.7. A quadrotor design offered the highest endurance of 5.4 hours, at the aspect ratio of 12.5 and radius of 0.178 m.

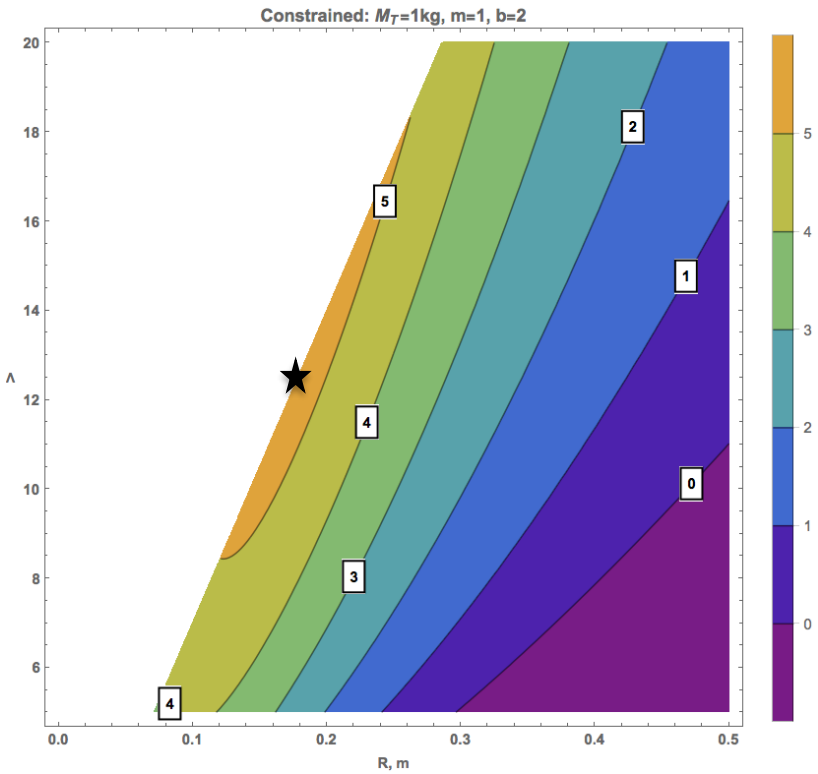

Figure 4.7: Hover endurance from Model 2 for M_T = 1kg, m=1, b=2

Quasi-quadrotor with M_T = 10kg: Figure 4.8 shows the contour plots obtained for a 10 kg QQ for a quadrotor design i.e., multiplicity, m=1. It is observed that with an increase in m value, endurance increases slightly until m=3 and then decreases. The endurance was found to be maximum at the upper limit of the blade aspect and the radius of 0.301 m. When compared to the previous case, the endurance value was increased by 1.33 hours.

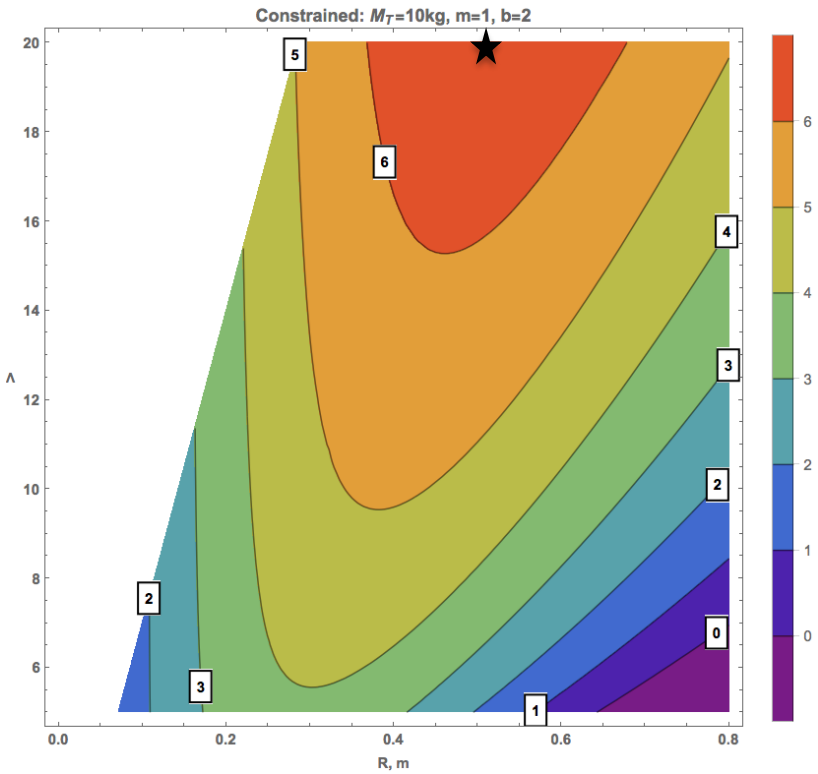

Figure 4.8: Hover endurance from Model 2 for M_T = 10kg, m=1, b=2

Quasi-quadrotor with M_T =10^2, 10^3, and 10^4 kg: Figures 4.9-4.14 shows the results obtained from the optimization study conducted considering 10^2, 10^3, and 10^4 kg MTOM. While the contour plots shown as Figs. 4.9, 4.11 and 4.13, respectively, show the dependence of endurance on the radius and the aspect ratio of the optimized propulsion pod, Figs. 4.10, 4.12, and 4.14 show the variation of the endurance with the multiplicity factor for 10^2, 10^3, and 10^4 kg QQ, respectively. It is the 10^4 kg QQ which benefited the most in distributing the propulsion.

It is observed that the radius of the rotor, the blade aspect ratio, and the endurance for all the three above mentioned QQ VTOL vehicles are equal. However, the optimized multiplicity factor varies.

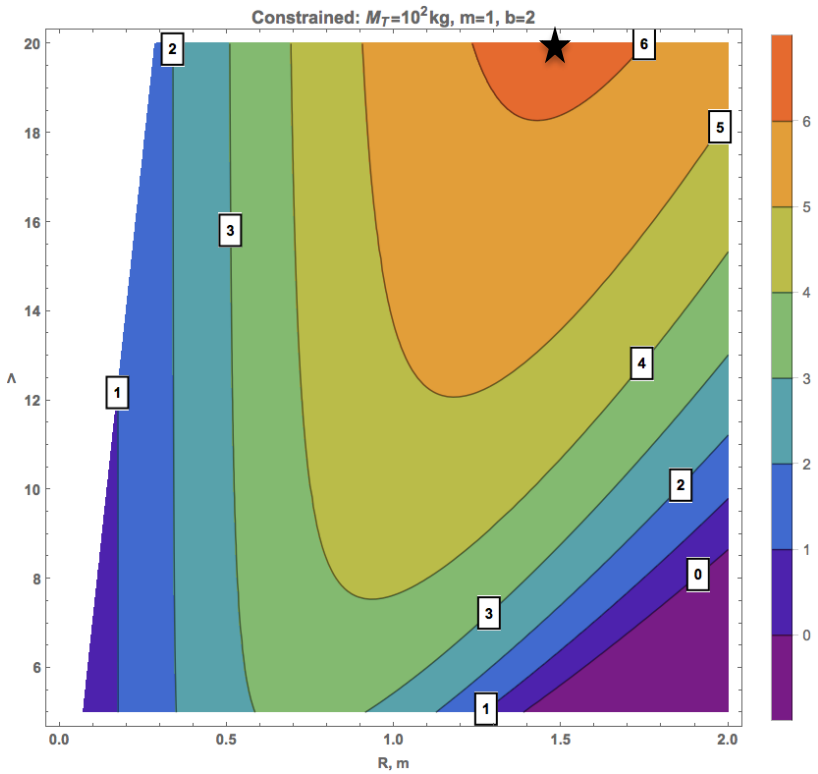

Figure 4.9: Hover endurance from Model 2 for $M_T = 10^2$ kg, m=1, b=2

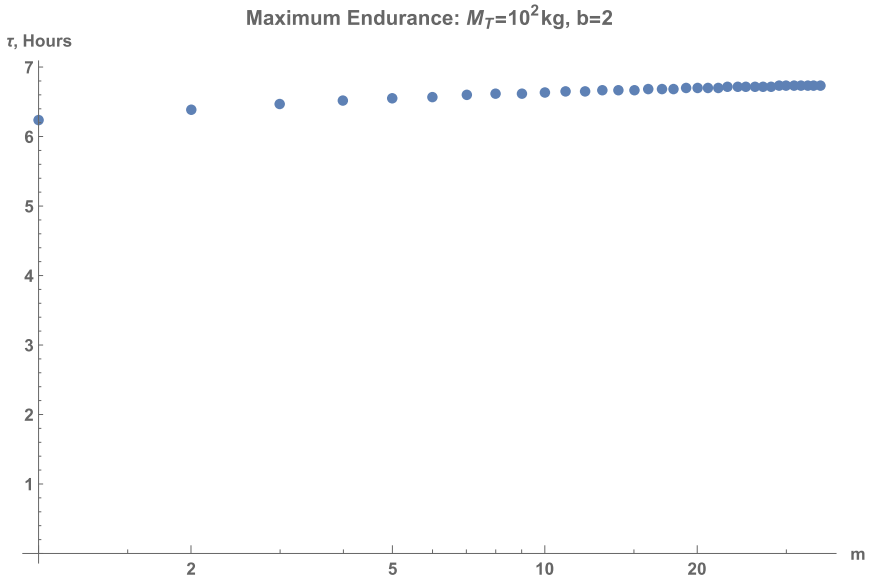

Figure 4.10: Endurance variation with multiplicity from Model 2 for $M_T = 10^2$kg

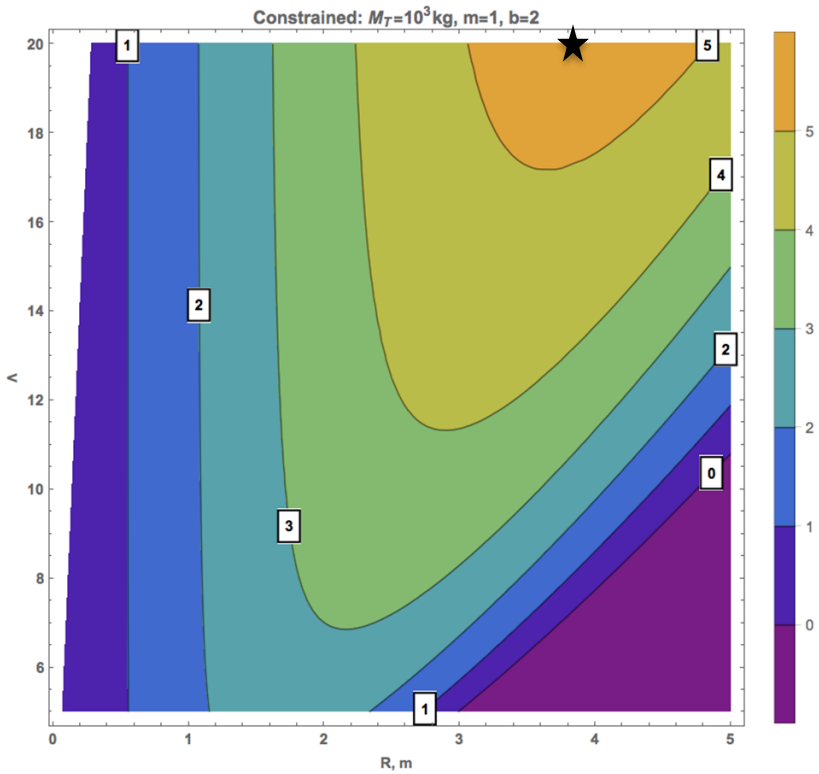

Figure 4.11: Hover endurance from Model 2 for $M_T = 10^3$ kg, m=1, b=2

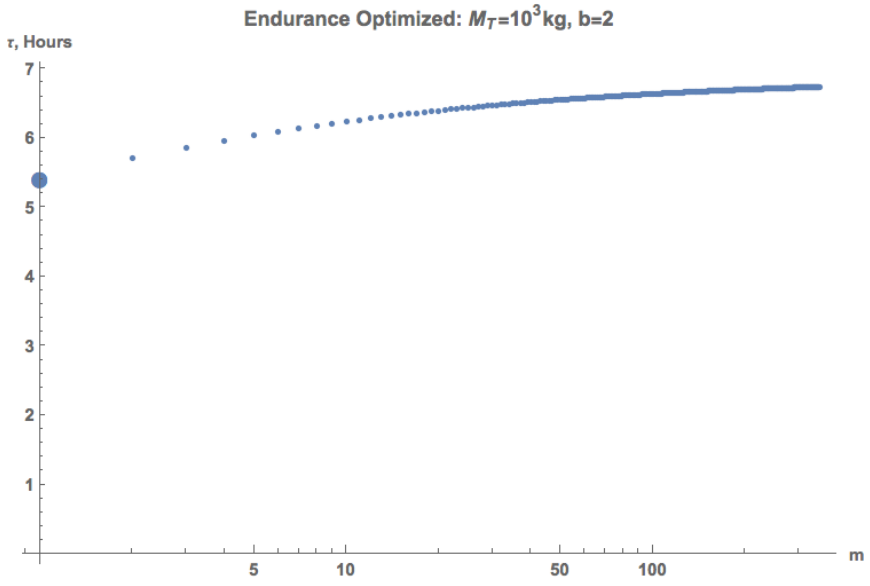

Figure 4.12: Endurance variation with multiplicity from Model 2 for $M_T = 10^3$kg

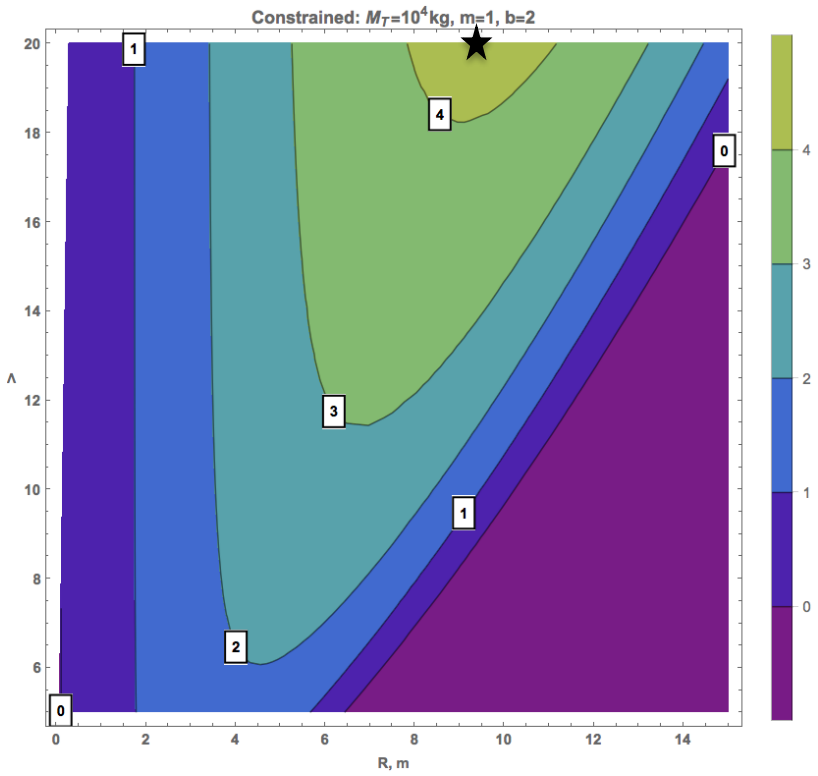

Figure 4.13: Hover endurance from Model 2 for $M_T = 10^4$ kg, m=1, b=2

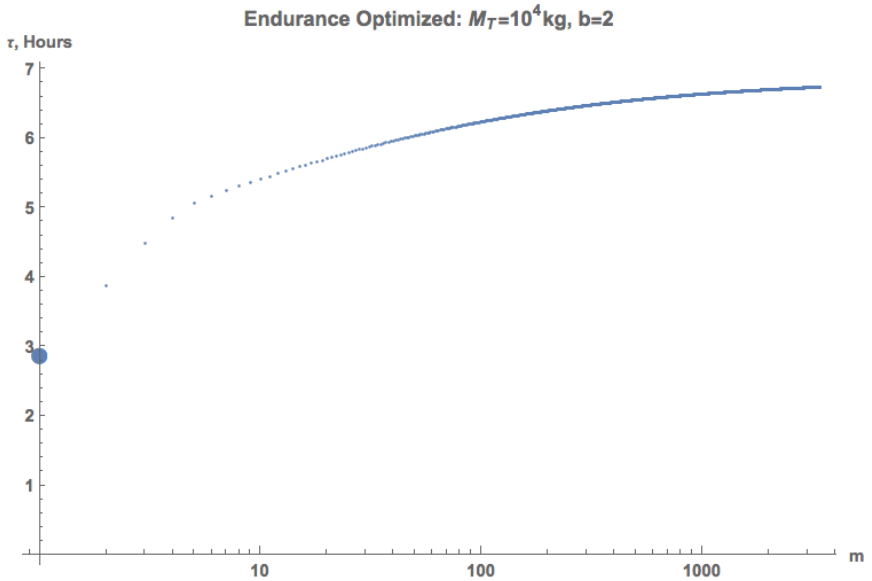

Figure 4.14: Endurance variation with multiplicity from Model 2 for $M_T = 10^4$kg

Table 4.1 summarizes the optimized endurance values for two bladed quasi-quadrotors using Model 2. At low total mass 10^{-1}kg, the blades with an aspect ratio of 5 provide the highest endurance and in contrast, a total mass greater than 10kg, the rotor blades with an aspect ratio of 20 provide the maximum endurance. However, the maximized endurance achievable at smaller M_T is very low when compared to higher M_T. Moreover, we observe that an endurance optimized pod exists (highlighted in the table), allowing any larger vehicle to be conceived by adding optimized pods in multiples of four, until the total weight desired, with no penalty in endurance. In addition, it is found that the optimized propulsor pod consists of more than 90% of battery by mass.

Table 4.1: Endurance optimized results summary from Model 2

M_T, kg	m	Λ	R, m	τ, Hours
10^{-1}	1	5	0.07153	2.02389
10^{0}	1	12.4765	0.17848	5.40025
10^{1}	3	20	0.30088	6.72681
10^{2}	34	20	0.28611	6.73393
10^{3}	339	20	0.28611	6.73396
10^{4}	3388	20	0.28611	6.73396

4.3.2 Model 3

Unlike Model 2, the power and the endurance calculation using Model 3 requires evaluation of algorithm described in the Fig. 3.3 coupled with SQP. The calculation of the power required to hover using Model 3, depends on six parameters:

1. Total vehicle mass, M_T

2. Multiplicity factor of quasi-quadrotor, m
3. Number of blades of rotor, b
4. Aspect ratio of the blades, Λ
5. Radius of the individual rotor, R and
6. Twist rate, θ_1

The propulsor blade is divided into N smaller elements of span Δr, and the differential thrust generated and power required are calculated. Leishman [] suggests a minimum of 20 elements need to be considered to ensure an adequate numerical resolution of the inflow and spanwise loading, but 40 elements or more is desirable.

Figure 4.15 shows the variation of the coefficient of thrust with a number of blade elements N. It is found that there is no significant change in the coefficient of thrust calculated when N is greater than 100. Therefore, for this study one hundred blade elements were used.

Considering linear twist distribution, the twist rate θ_1 has been varied from -50 °/r to 0 °/r in an increment of 0.25 °/r, while correction the geometric root pitch θ_0 to satisfy hover conditions. It is found that there exists a twist rate for which the hover endurance is maximum.

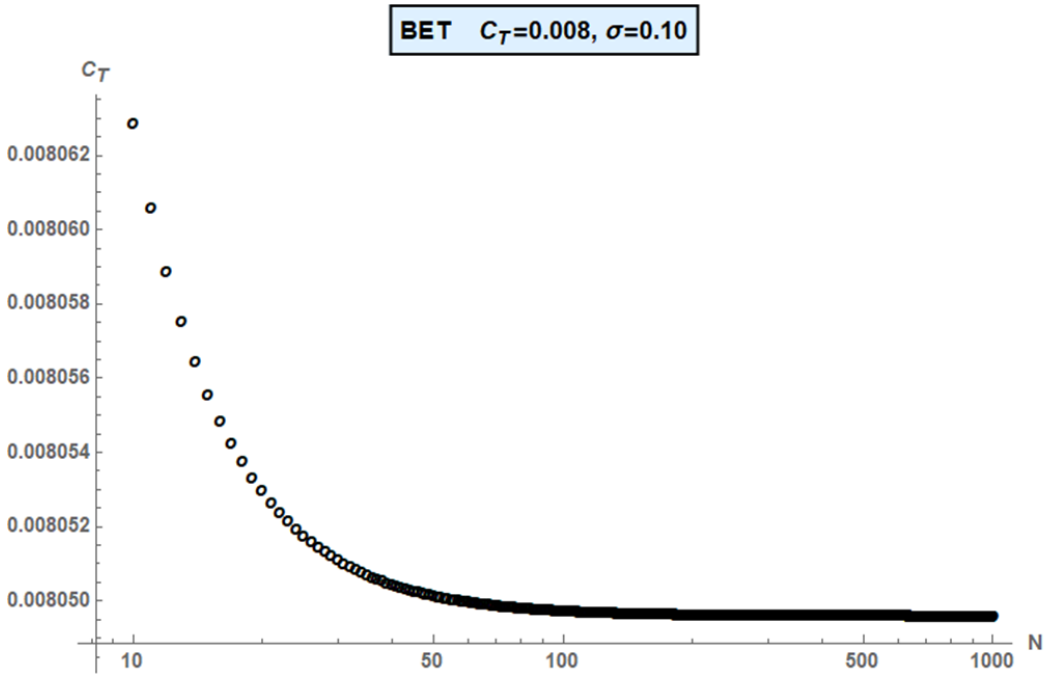

Figure 4.15: Variation of calculated thrust coefficient with number of blade elements

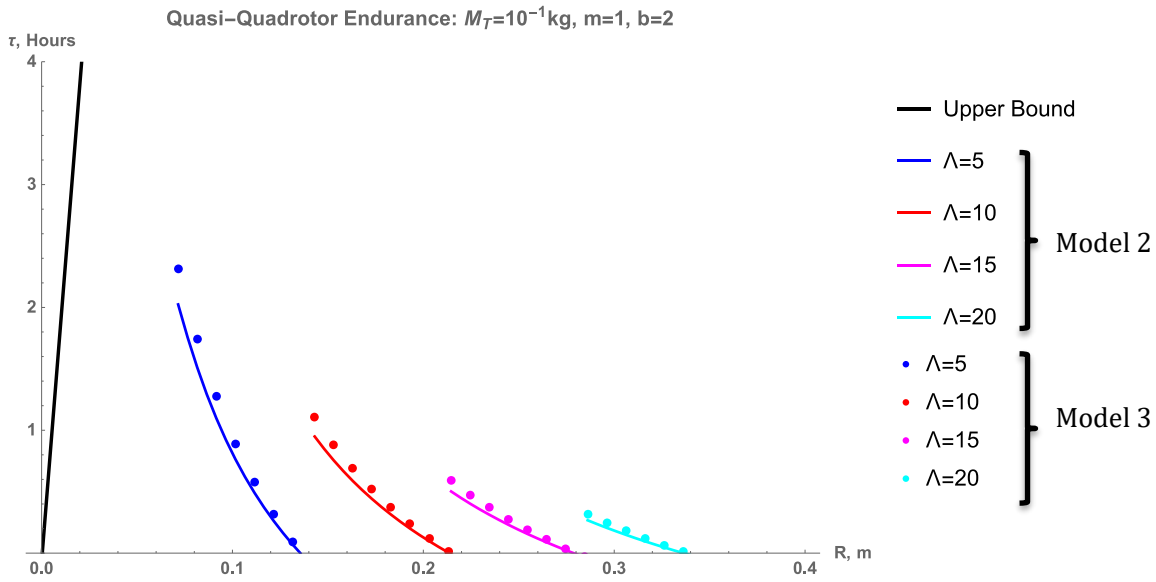

Figure 4.16: Endurance comparison for M_T = 10^{-1} kg, m=1, b=2

Limiting the scaling investigation to two bladed rotors with the blade aspect ratio varying from 5 to 20, optimization is carried out across several orders of magnitude of M_T by varying individual pod radius and multiplicity factor. Figure 4.16 shows the endurance comparison using Model 1, 2, and 3 across the aspect ratios of 5, 10, 15, and 20.

It is observed that there is a slight increase in hover endurance obtained by Model 3, as the blade element theory allows the inclusion of the distribution of twist. Consequently, for the given blade aspect ratio and radius, higher endurance values can be obtained leveraging the advantages of twisted blades.

Quasi-quadrotor with M_T = 10^{-1}kg: Contours of the hover endurance are obtained using the evaluation points as illustrated in Fig. 4.17. As observed in Model 2 due to the low tip Reynolds number, the endurance is decreased with an increase in the blade aspect ratio. Dependence of endurance on aspect ratio and blade radius is summarized in Fig. 4.18. The maximum value of endurance is obtained at the lower limit of the blade aspect ratio. Additionally, a further increase in m values had adverse effects on the endurance, suggesting that a quadrotor at the lower limit of the considered aspect ratio resulted in the maximum endurance of 2.31 hours.

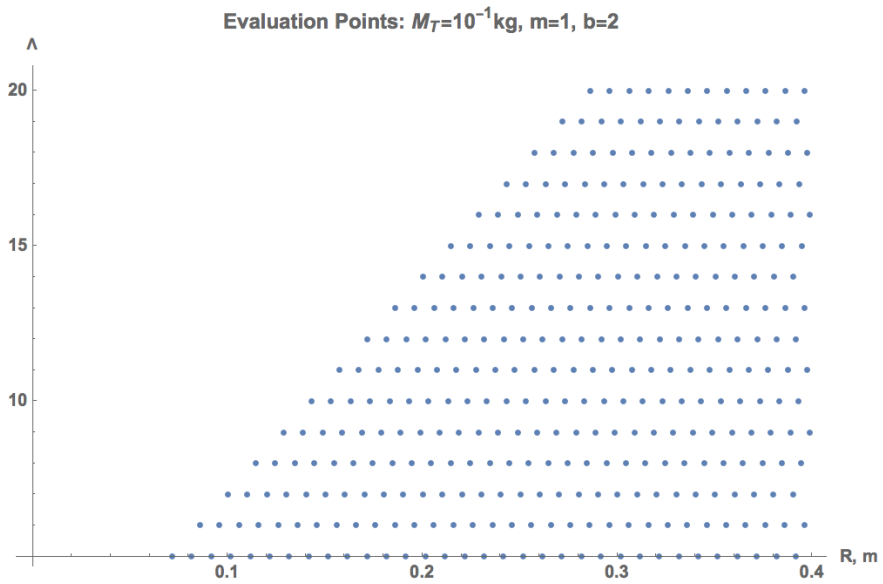

Figure 4.17: Endurance evaluation points for $M_T = 10^{-1}$ kg, m=1, b=2

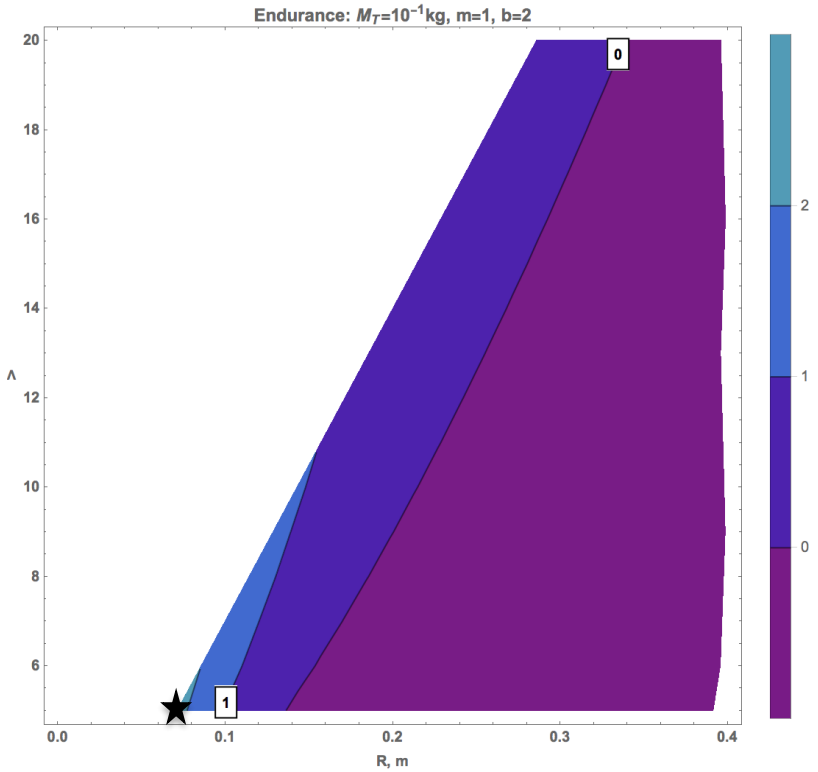

Figure 4.18: Hover endurance from Model 3 for $M_T = 10^{-1}$ kg, m=1, b=2

Quasi-quadrotor with M_T = 1kg: Repeating the constrained study at one-kilogram mass resulted in a contour plot as illustrated in Figs. 4.19. A quadrotor design offered the highest endurance of 5.86 hours, at the aspect ratio of 13.76 and a radius of 0.197 m.

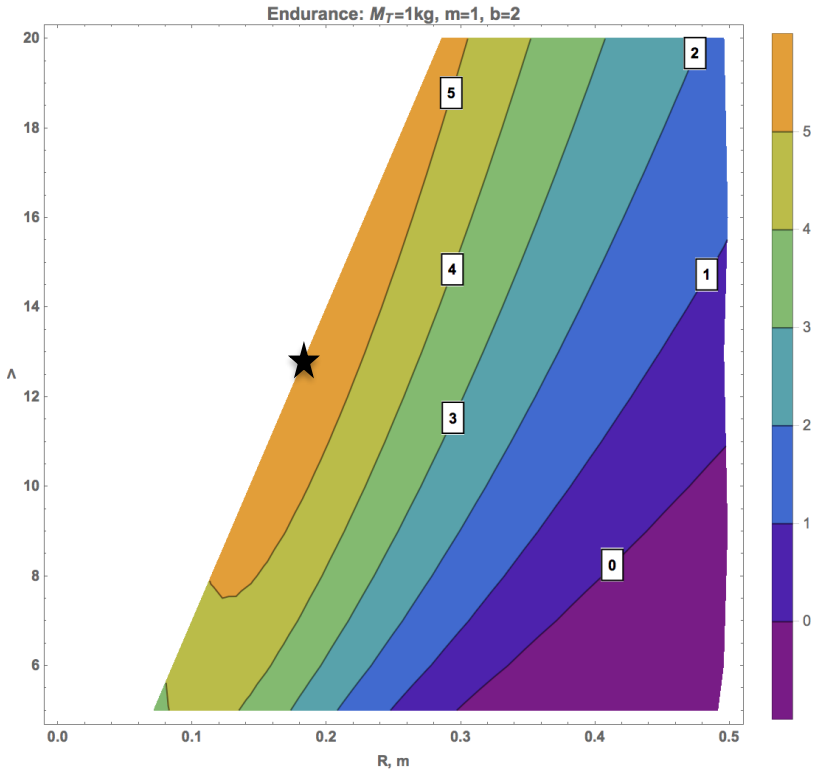

Figure 4.19: Hover endurance from Model 3 for M_T = 1 kg, m=1, b=2

Quasi-quadrotor with M_T = 10kg: Figure 4.20 shows the results of the optimization performed for a 10 kg QQ at various aspect ratios. It is observed that with an increase in m value, endurance increases slightly until m=4 and then decreases. The endurance was found to be maximum at the upper limit of the blade aspect and the radius of 0.288 m.

Quasi-quadrotor with M_T =10^2, 10^3, and 10^4 kg: Figures 4.21-4.26 shows the results obtained from the optimization study conducted considering 10^2, 10^3, and 10^4 kg MTOM. While the contour plots shown as Figs. 4.21, 4.22 and 4.23, respectively, show the dependence of endurance on the radius and the aspect ratio of the optimized propulsion pod, Figs. 4.24, 4.25, and 4.26 show the variation of the endurance with the multiplicity factor for 10^2, 10^3, and 10^4 kg QQ, respectively. It is observed that the radius of the rotor, the blade aspect ratio, and the endurance for all the three above mentioned QQ VTOL vehicles are equal. However, the optimized multiplicity factor varies.

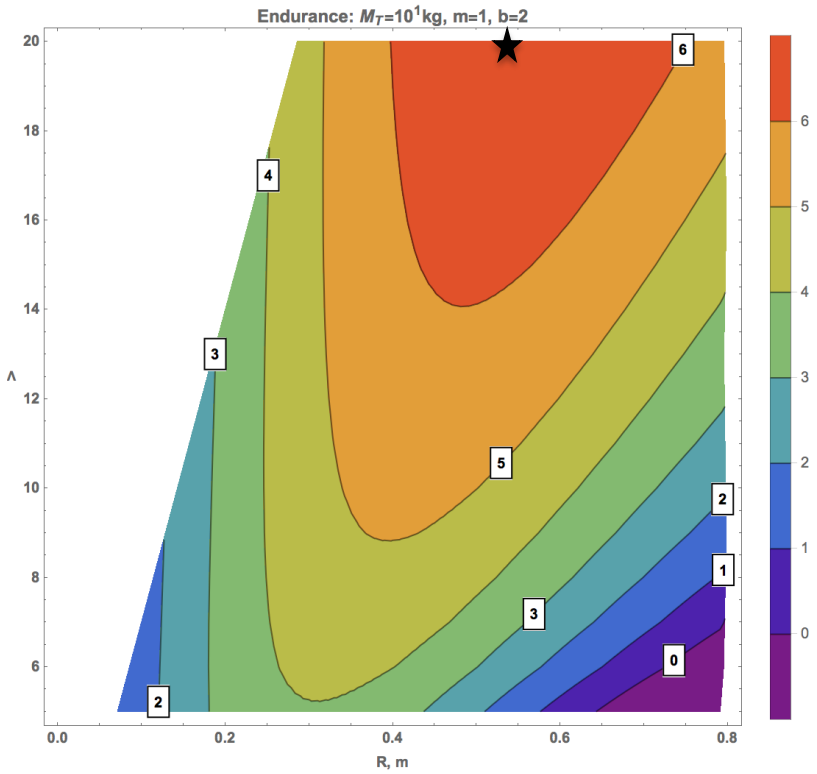

Figure 4.20: Hover endurance from Model 3 for M_T = 10 kg, m=1, b=2

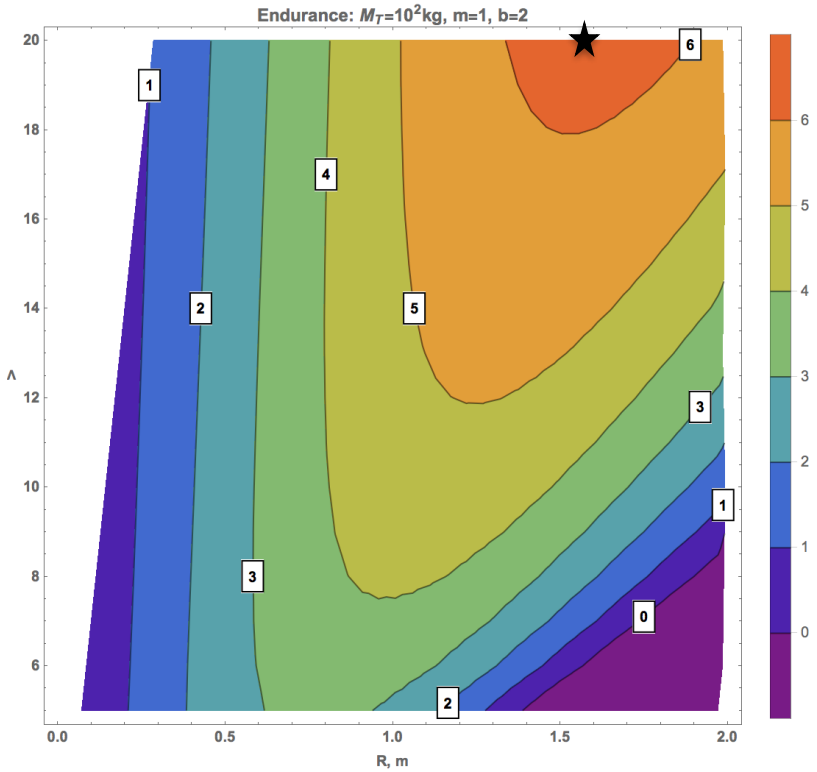

Figure 4.21: Hover endurance from Model 3 for M_T = 10^2 kg, m=1, b=2

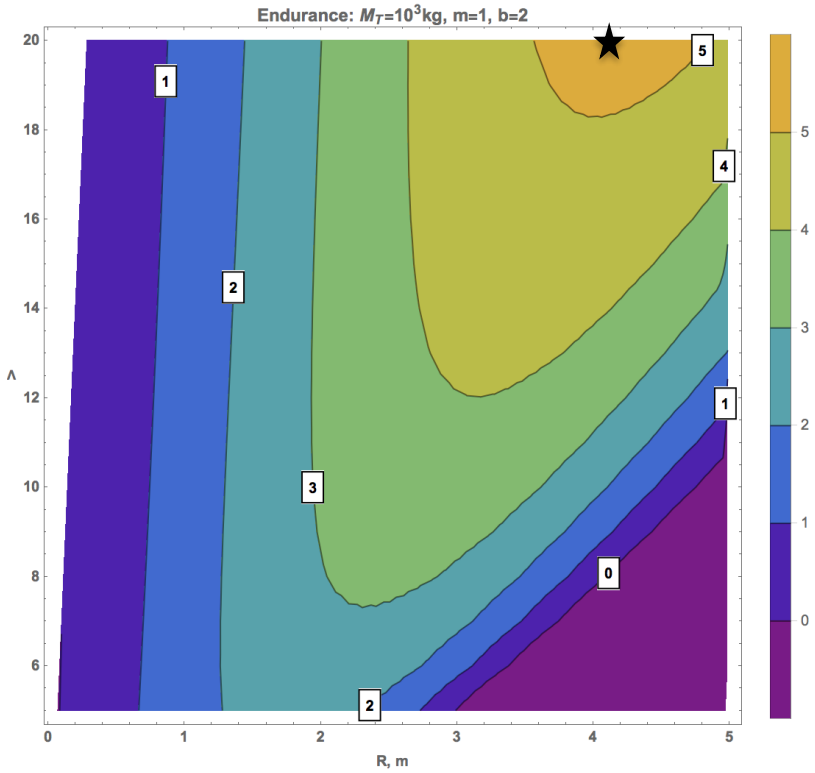

Figure 4.22: Hover endurance from Model 3 for $M_T = 10^3$ kg, m=1, b=2

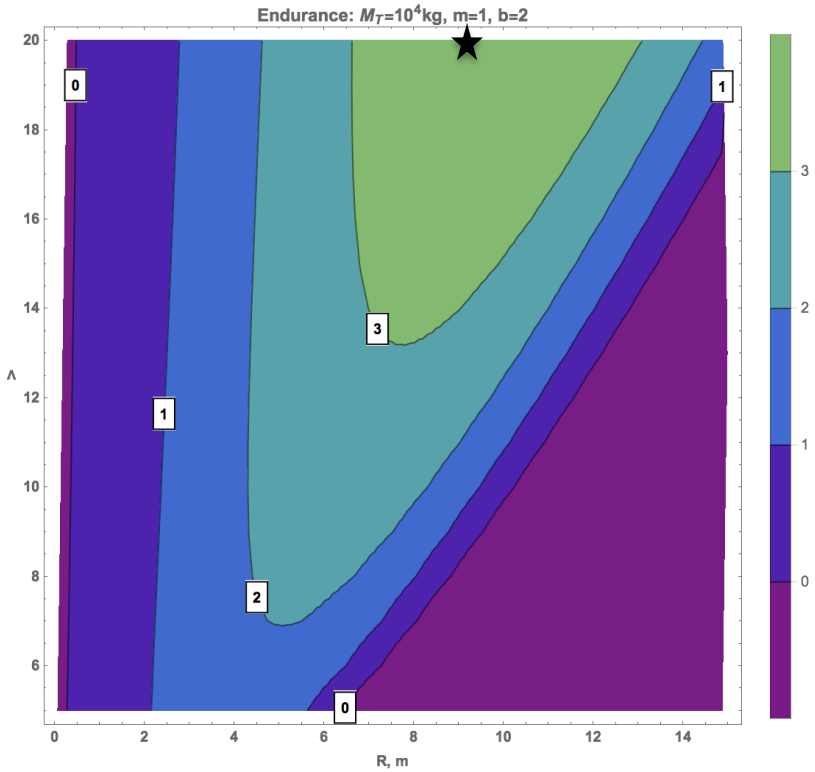

Figure 4.23: Hover endurance from Model 3 for $M_T = 10^4$ kg, m=1, b=2

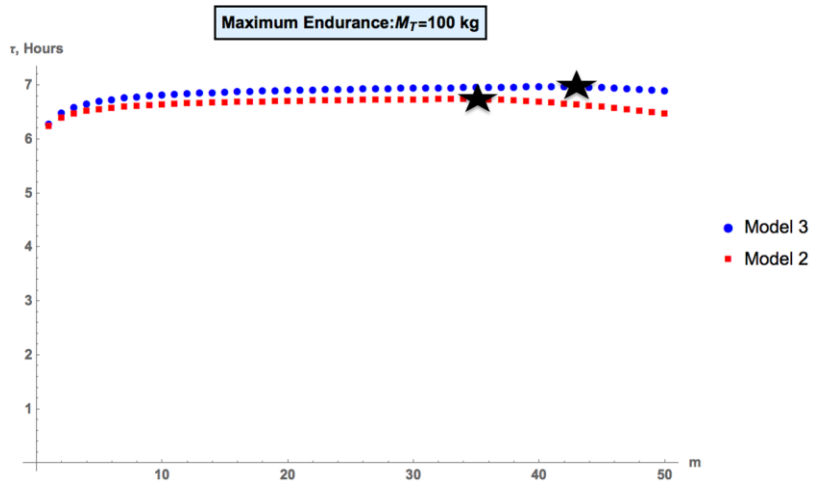

Figure 4.24: Endurance variation with multiplicity from Model 2 and 3 for $M_T = 10^2$kg

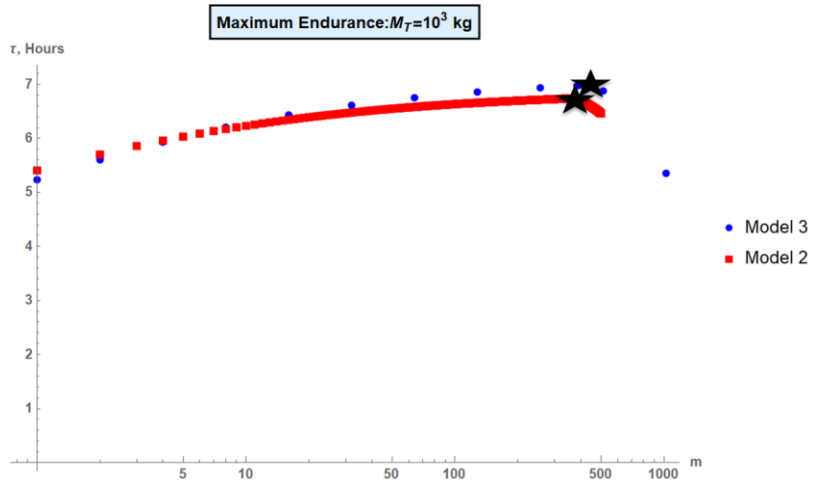

Figure 4.25: Endurance variation with multiplicity from Model 2 and 3 for $M_T = 10^3$kg

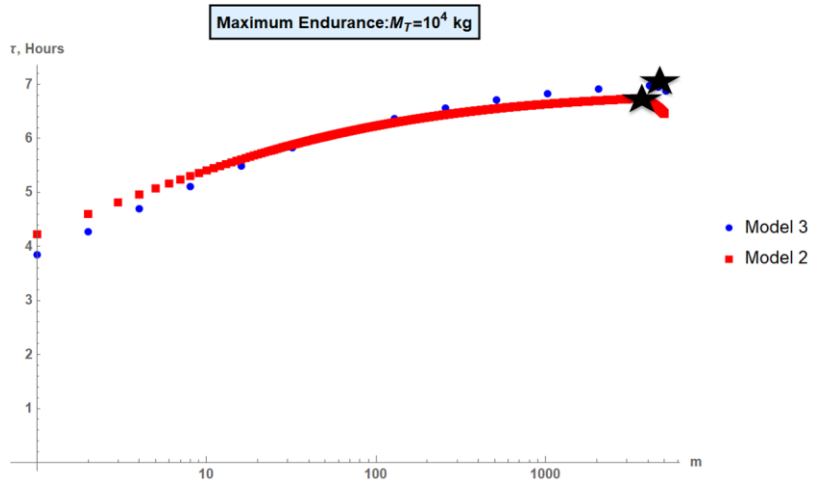

Figure 4.26: Endurance variation with multiplicity from Model 2 and 3 for $M_T = 10^4$kg

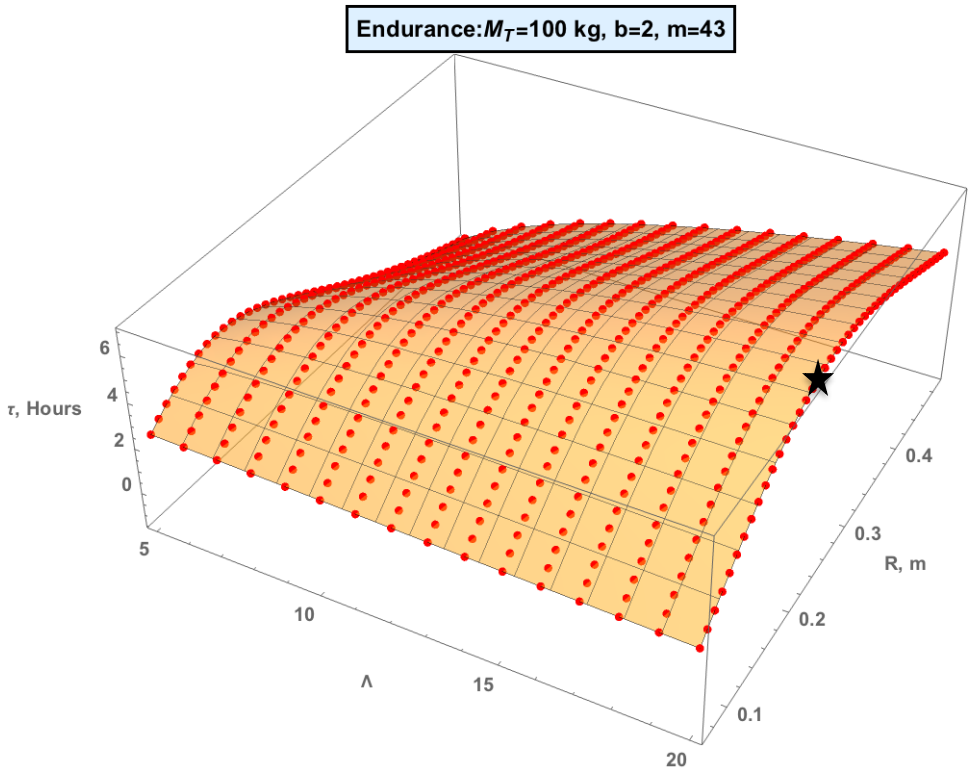

Figure 4.27: Evaluation points and surface interpolation for $M_T = 10^2$ kg, m=43, b=2

The maximum hover endurance is numerically calculated, Fig. 4.27 illustrates the data points (shown in red) for which the endurance is evaluated and the interpolated surface. The hover endurance calculated using Model 3 for 10^2 kg QQ is maximum when the multiplicity is 42, the aspect ratio is 20 and the rotor radius is 0.28611. As observed in Table 4.1, hover endurance estimated from Model 3 for 10^2 kg QQ is also maximum where both the Reynolds number and the aspect ratio constraints are active.

Table 4.2 summarizes the optimized endurance values for two bladed quasi-quadrotors using Model 2. At low total mass 10^{-1}kg, the blades with an aspect ratio of 5 provide the highest endurance and in contrast, a total mass greater than 10kg, the rotor blades with an aspect ratio of 20 provide the maximum endurance. However, the maximized endurance achievable at smaller M_T is very low when compared to higher M_T. Moreover, we observe that an endurance optimized pod exists (highlighted

in the table), allowing any larger vehicle to be conceived by adding optimized pods in multiples of four, until the total weight desired, with no penalty in endurance.

Table 4.2: Endurance optimized results summary using Model 3

M_T, kg	m	Λ	R, m	τ, Hours
10^{-1}	1	5	0.07153	2.31590
10^{0}	1	13.7542	0.19676	5.85690
10^{1}	4	20	0.28766	6.97648
10^{2}	42	20	0.28611	6.97743
10^{3}	413	20	0.28611	6.97743
10^{4}	4127	20	0.28611	6.97743

4.3.3 Model 4

For the calculation of the power required to hover using Model 4, seven parameters were considered:

1. Total vehicle mass, M_T
2. Multiplicity factor of quasi-quadrotor, m
3. Number of blades of rotor, b
4. Aspect ratio of the blades, Λ
5. Radius of the individual rotor, R
6. Twist rate, θ_1 and
7. Taper ratio, TR

As explained in section 4.3.2, the propulsor blade is divided into 100 smaller elements of span Δr, and the differential thrust generated and power required are calculated to ensure an adequate numerical resolution of the inflow and spanwise loading.

Linear twist distribution was considered and the twist rate θ_1 has been varied from -50 °/r to 0 °/r in an increment of 0.25 °/r, while correction the geometric root pitch θ_0 to satisfy hover conditions. The scaling investigation was limited to two bladed rotors with the blade aspect ratio varying from 5 to 20, optimization is carried out across several orders of magnitude of M_T by varying individual pod radius, blade aspect ratio, multiplicity factor, blade twist distribution, and taper ratio.

Furthermore, the MATLAB® code was verified by reproducing the numerical results obtained by Leishman [36], and by comparing numerically predicted values to experimental data obtained by Castles and Gray [41].

Figure 4.28 describes the variation of thrust gradient of a rotor with a thrust gradient of 0.008 and a solidity ratio of 0.10, for two twist rates. Figure 4.29 illustrates the variation of the local lift coefficient with a normalized radius for three taper ratios considering tip losses. Figure 4.30 shows the variation of thrust gradient of an untwisted rectangular blade, with and without considering tip loss.

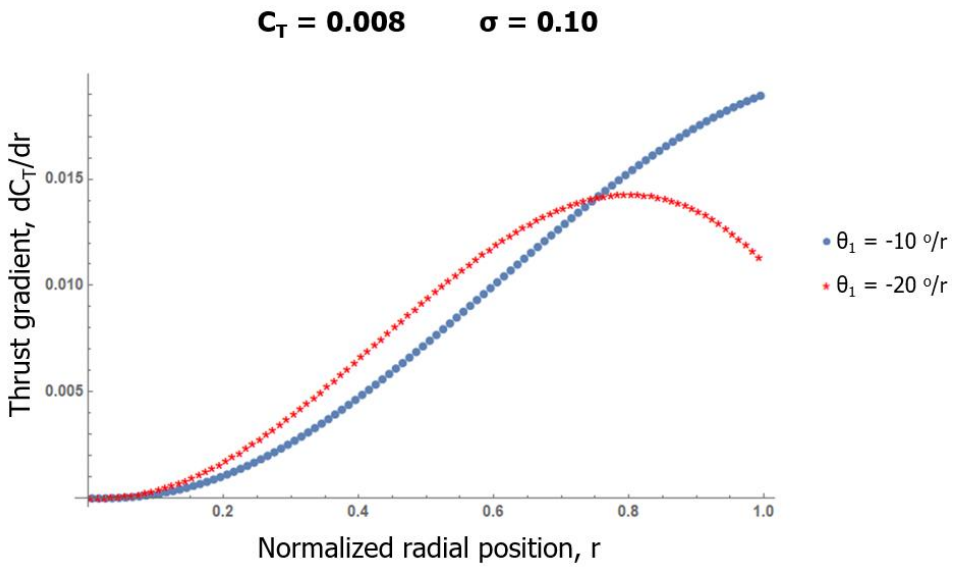

Figure 4.28: Variation of thrust gradient with a normalized radius [36]

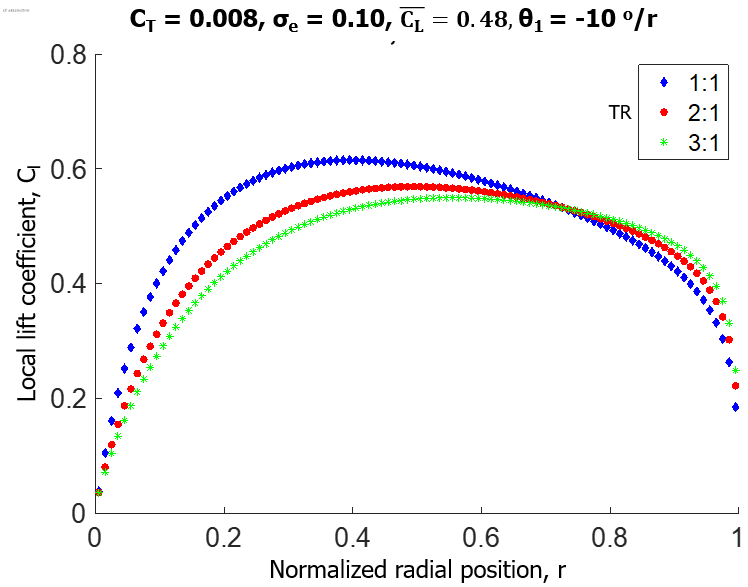

Figure 4.29: Variation of local lift coefficient with a normalized radius [36]

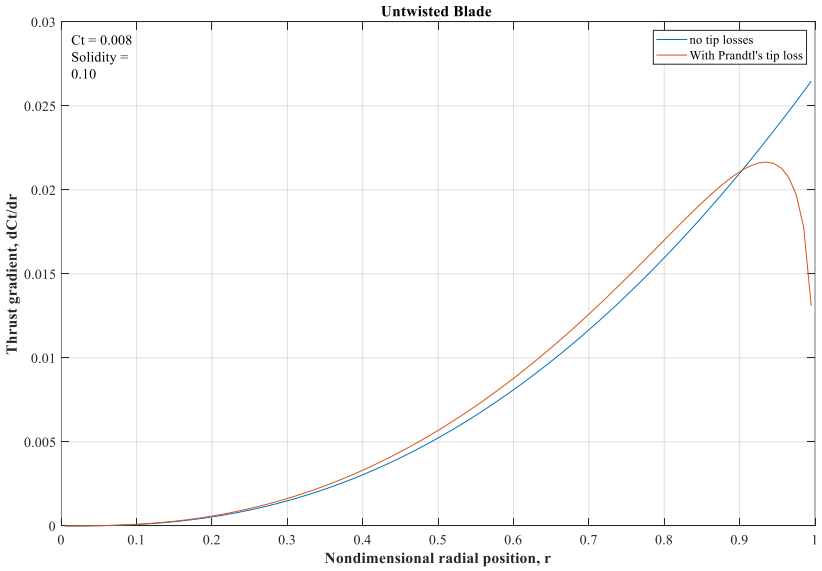

Figure 4.30: Variation of thrust gradient with normalized radius considering tip losses [36]

Castles and Gray [41] measured the coefficient of thrust for a 6ft diameter rotor with untwisted blades of different taper ratios. Figures 4.31 and 4.32, shows the variation of coefficient of thrust with twist measured at 75% radius, for rotor blades with a taper ratio of 1 and 0.33, respectively. Predicted thrust coefficient values show good correlation with experimentally measured data.

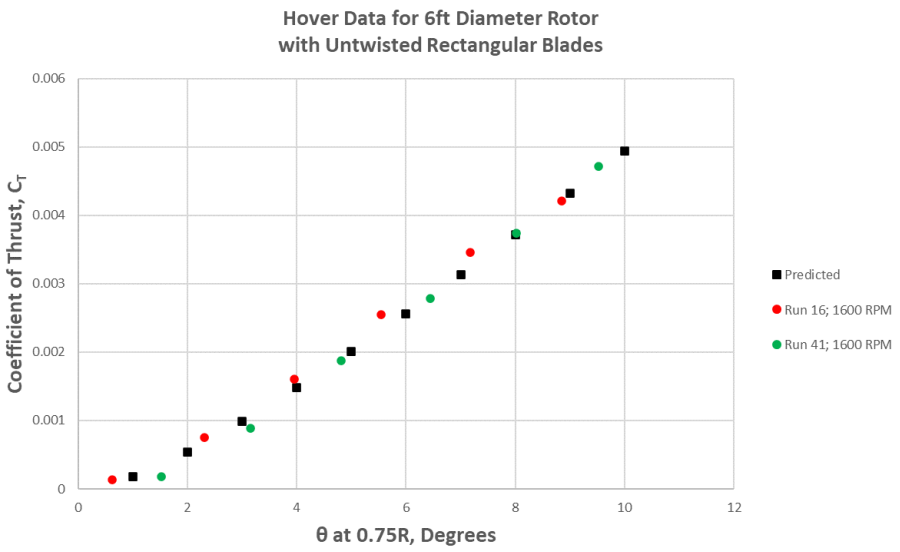

Figure 4.31: Variation of thrust coefficient with twist for rectangular blades

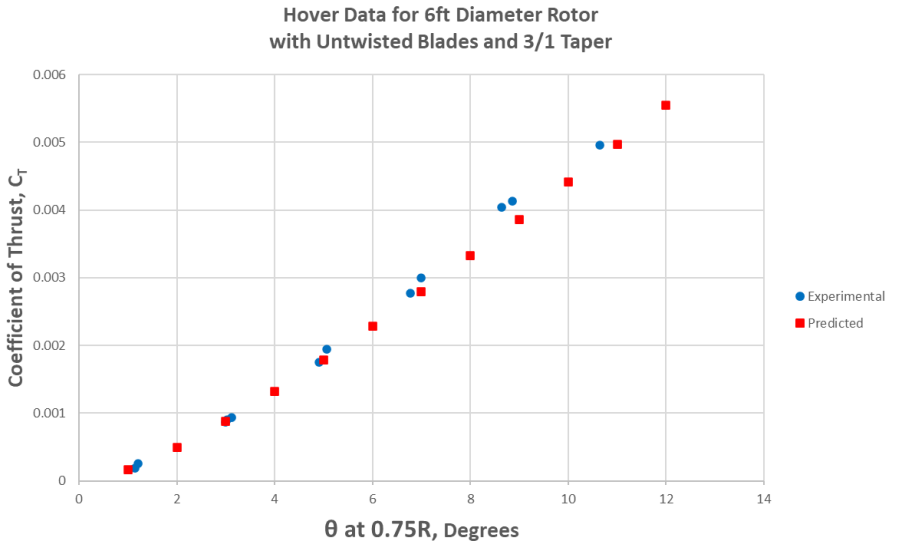

Figure 4.32: Variation of thrust coefficient with twist for tapered blades

<u>Quasi-quadrotor with $M_T = 10^{-1}$kg:</u> As observed in Model 2 due to the low tip Reynolds number, the endurance is decreased with an increase in the blade aspect ratio. Dependence of endurance on aspect ratio is summarized in Fig. 4.33. The maximum value of endurance is obtained at the lower limit of the blade aspect ratio.

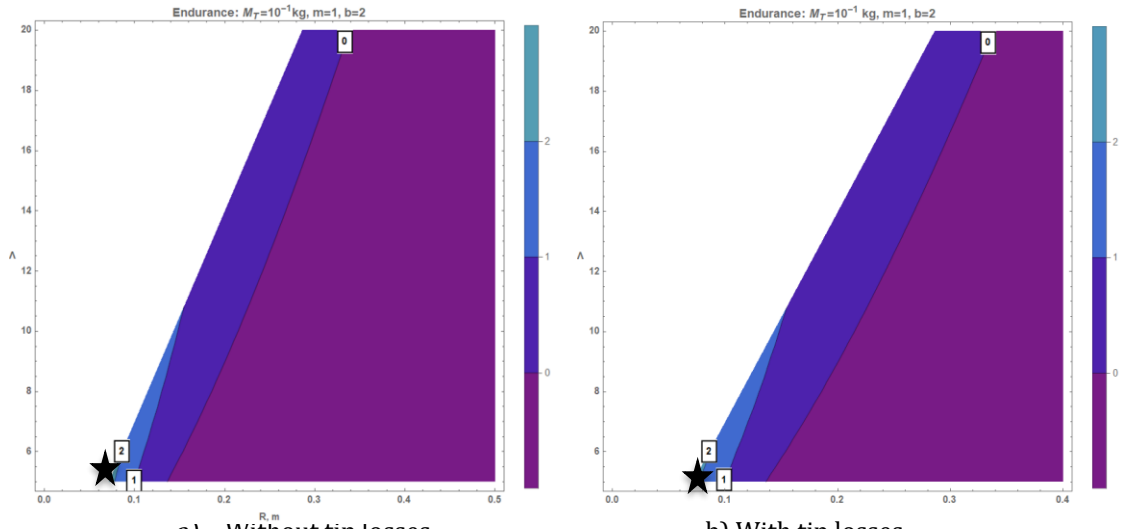

a) Without tip losses b) With tip losses

Figure 4.33: Hover endurance from Model 4 for $M_T = 10^{-1}$ kg, m=1, b=2, TR=1

Additionally, a further increase in m values and a decrease in taper ratio had adverse effects on the endurance, suggesting that a quadrotor with rectangular blades at the lower limit of the considered aspect ratio resulted in the maximum endurance of 2.81 hours considering tip losses.

Table 4.3: Variation of optimized endurance for $M_T = 10^{-1}$ kg, from Model 4 considering tip losses

TR	m	Λ	R, m	τ, Hours
1	1	5	0.07153	2.81309
0.8	1	5	0.08047	2.23213
0.6	1	5	0.09537	1.44761

Quasi-quadrotor with M_T = 1kg: Repeating the constrained study at one-kilogram mass resulted in a contour plot as illustrated in Fig.4.34. A quadrotor with rectangular blades offered the highest endurance of 6.17 hours, at the aspect ratio of 13.05 and radius of 0.187 m. Variation of endurance with taper ratio is presented in table 4.4.

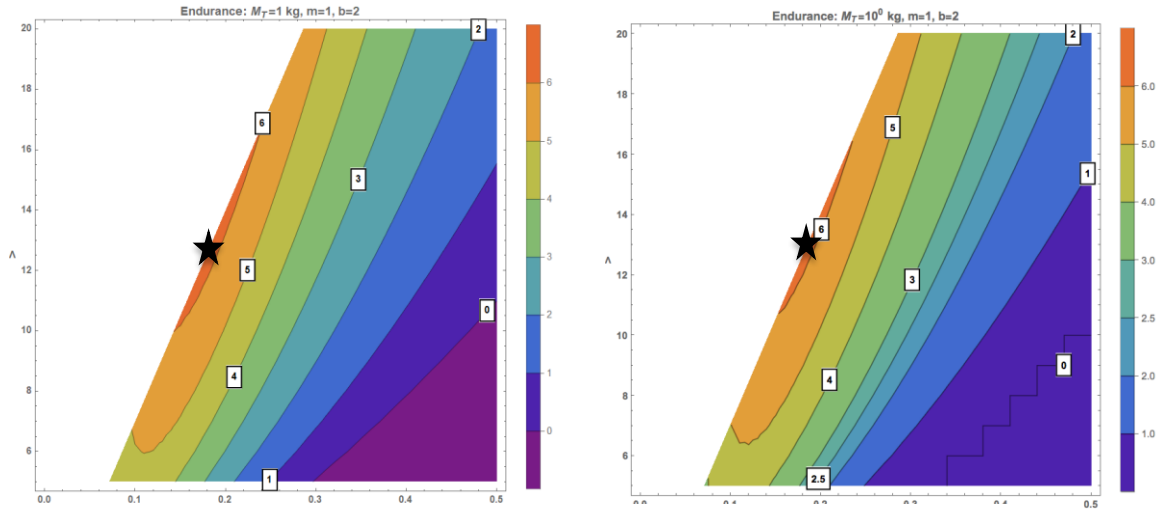

b) Without tip losses b) With tip losses

Figure 4.34: Hover endurance from Model 4 for $M_T = 10^0$ kg, m=1, b=2, TR=1

Table 4.4: Variation of optimized endurance for $M_T = 10^0$ kg, from Model 4 considering tip losses

TR	m	Λ	R, m	τ, Hours
1	1	13.054	0.18674	6.16588
0.8	1	11.197	0.18020	5.96807
0.6	1	9.0136	0.17192	5.64891

Quasi-quadrotor with M_T = 10kg: Figure 4.35 shows the results of the optimization performed for a 10 kg QQ at various aspect ratios. It is observed that with an increase in m value, endurance increases slightly and then decreases for rectangular blades. Although, as the taper ratio is decreased the endurance optimized multiplicity decreases suggesting that a quadrotor design with moderately tapered blades offers the highest endurance. In addition, as the taper ratio is decreased the endurance optimized radius values also increase. Table 4.5 shows the variation of optimized endurance with taper ratio.

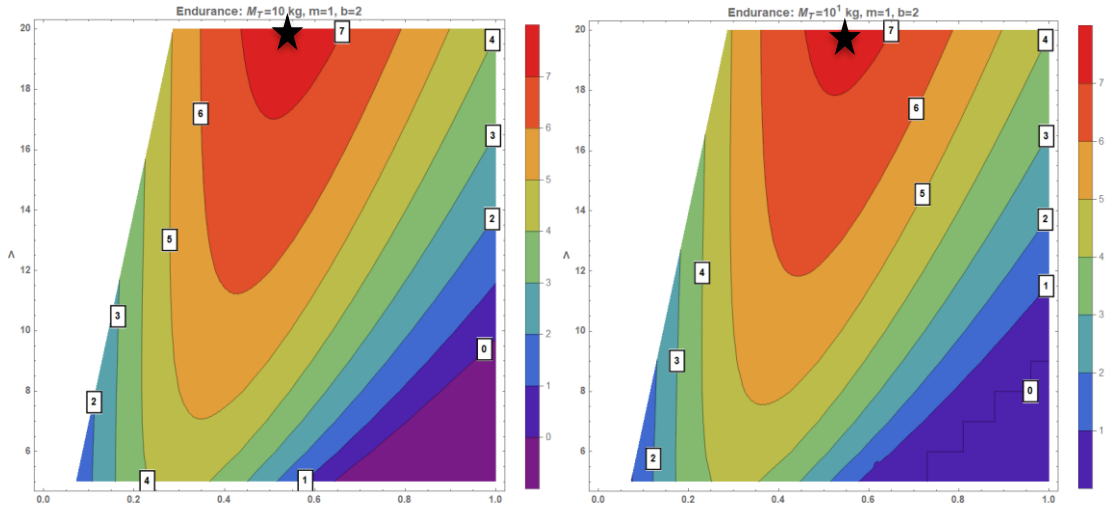

c) Without tip losses b) With tip losses

Figure 4.35: Hover endurance from Model 4 for $M_T = 10^1$ kg, m=1, b=2, TR=1

Table 4.4: Variation of optimized endurance for $M_T = 10^1$ kg, from Model 4 considering tip losses

TR	m	Λ	R, m	τ, Hours
1	4	20	0.28611	7.44687
0.8	3	20	0.32884	7.59107
0.6	2	20	0.41210	7.64997
0.4	1	20	0.59261	7.93834
0.2	1	16.4374	0.70542	7.23339

Quasi-quadrotor with $M_T = 10^2$, 10^3, and 10^4 kg: Figures 4.36-4.49 shows the results obtained from the optimization study conducted considering 10^2, 10^3, and 10^4 kg MTOM. While the contour plots shown as Figs. 4.36, 4.37 and 4.38, respectively, show the dependence of endurance on the radius and the aspect ratio of the quadrotor design, Figs. 4.39, 4.40, and 4.41 show the variation of the endurance with the multiplicity factor for 10^2, 10^3, and 10^4 kg QQ, respectively.

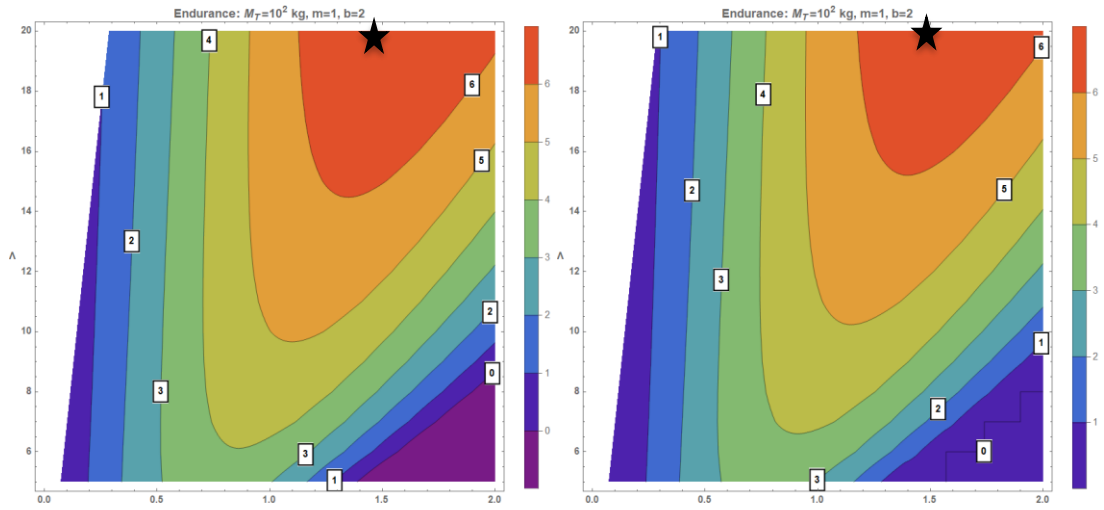

d) Without tip losses b) With tip losses

Figure 4.36: Hover endurance from Model 4 for $M_T = 10^2$ kg, m=1, b=2

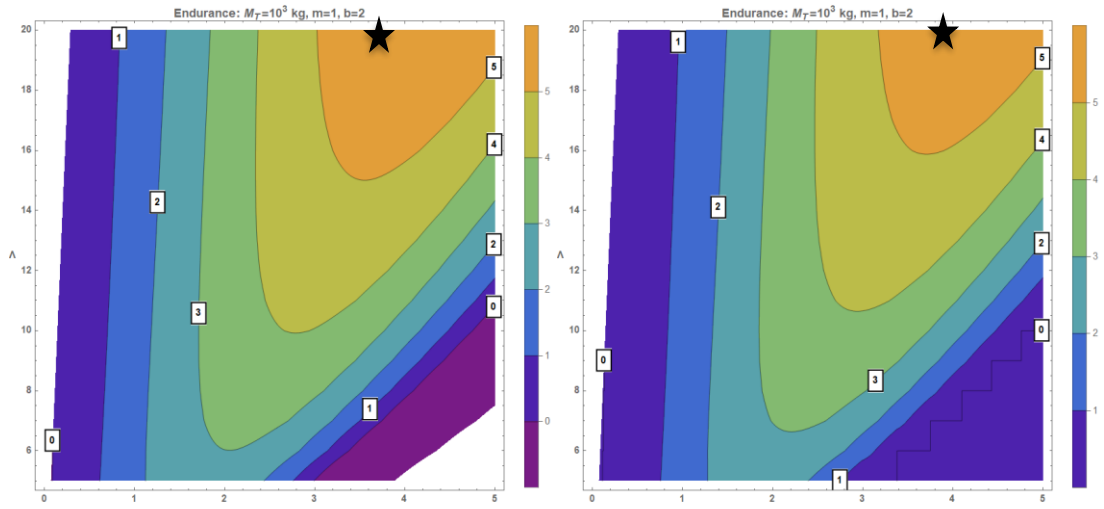

e) Without tip losses b) With tip losses

Figure 4.37: Hover endurance from Model 4 for $M_T = 10^3$ kg, m=1, b=2

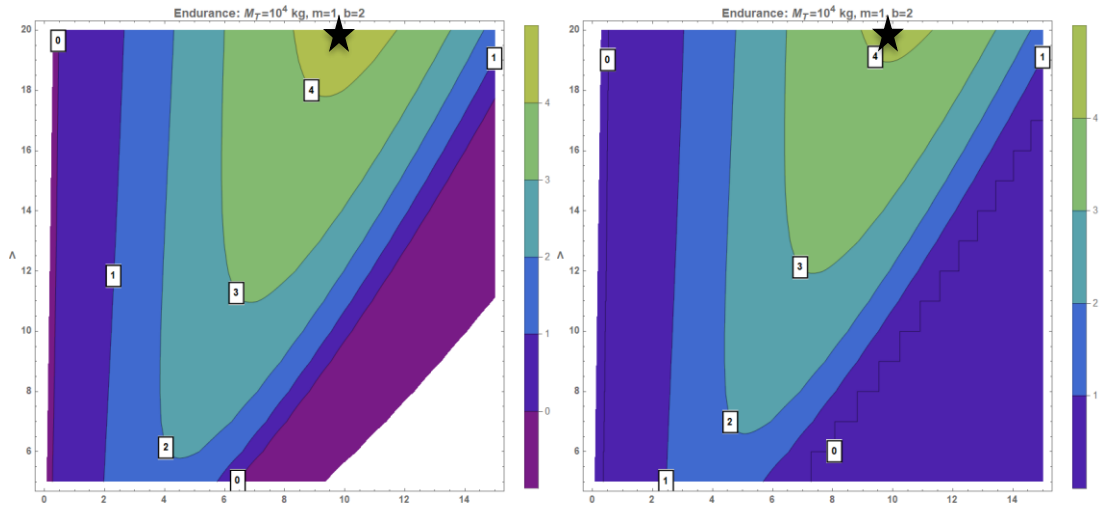

f) Without tip losses b) With tip losses

Figure 4.38: Hover endurance from Model 4 for $M_T = 10^4$ kg, m=1, b=2

It is observed that the endurance optimized radius of the rotor, the blade aspect ratio, and the endurance for all the three above mentioned QQ VTOL vehicles are equal. However, the optimized multiplicity factor varies. As seen in Figs. 4.39, 4.40, and 4.41 Model 3 underestimate the optimized endurance, whereas Model 4 without considering tip losses overestimates the endurance.

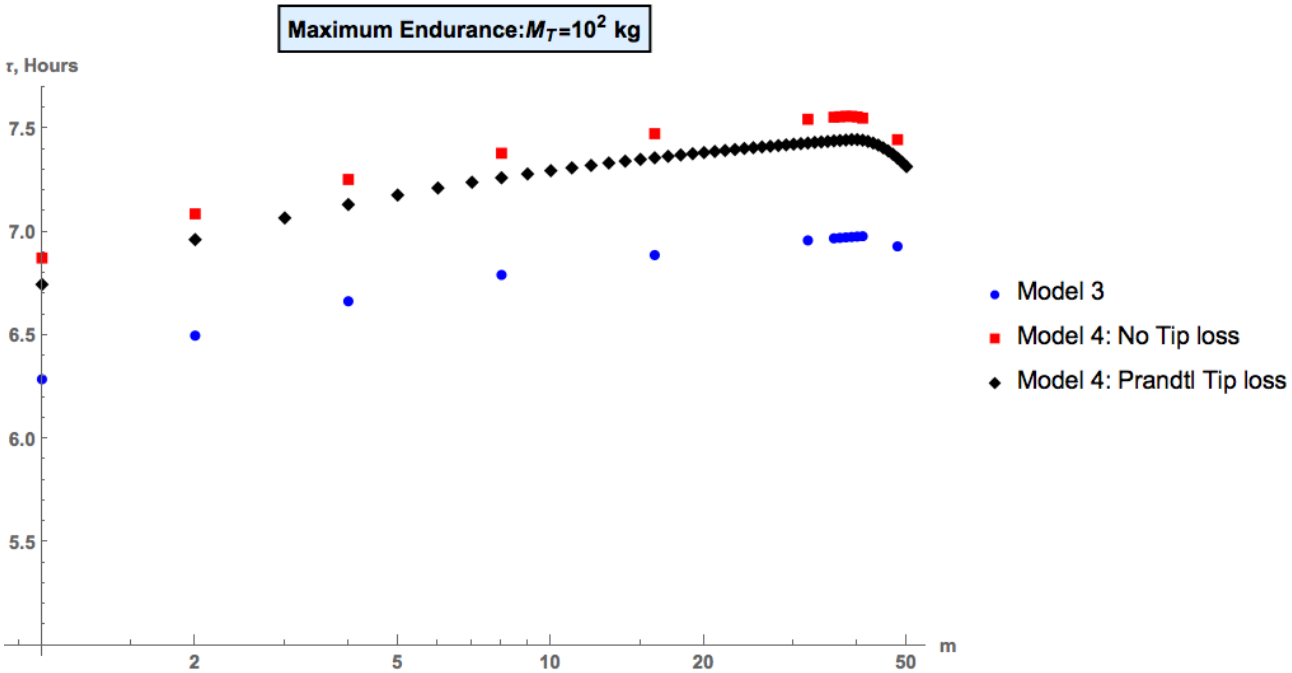

Figure 4.39: Endurance variation with multiplicity from Model 3 and 4 for $M_T = 10^2$kg, b=2, TR=1

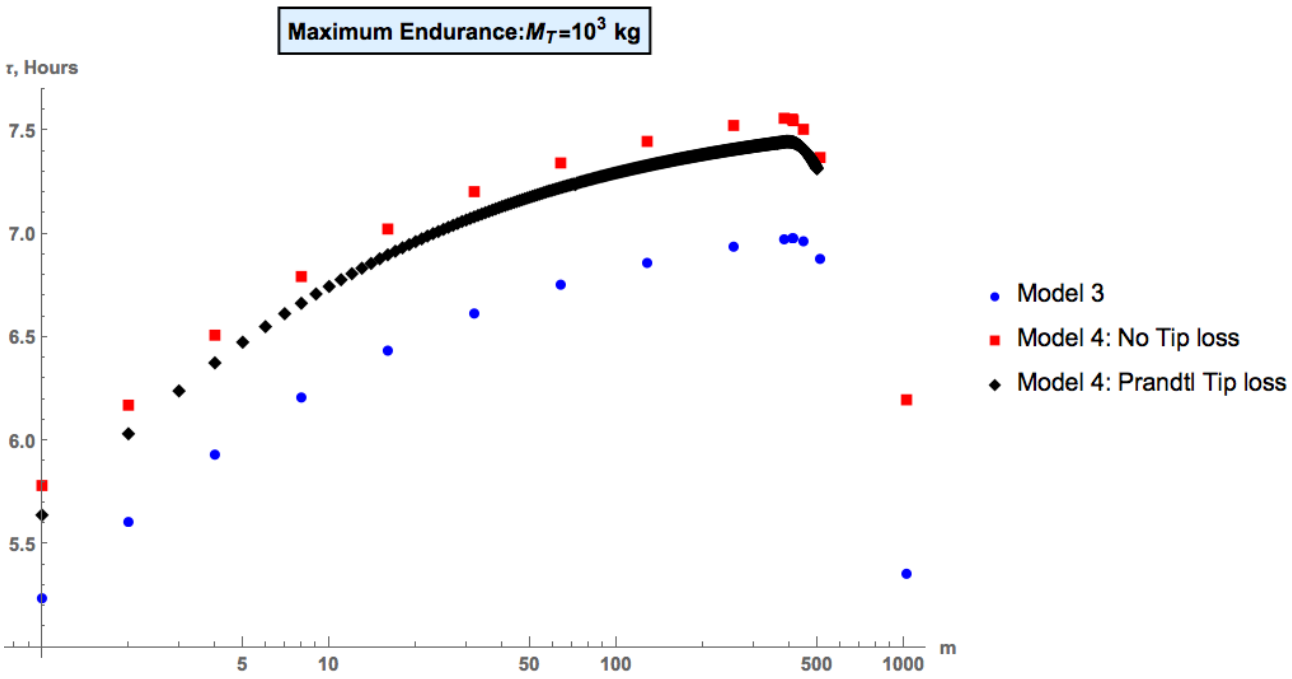

Figure 4.40: Endurance variation with multiplicity from Model 3 and 4 for $M_T = 10^3$kg, b=2, TR=1

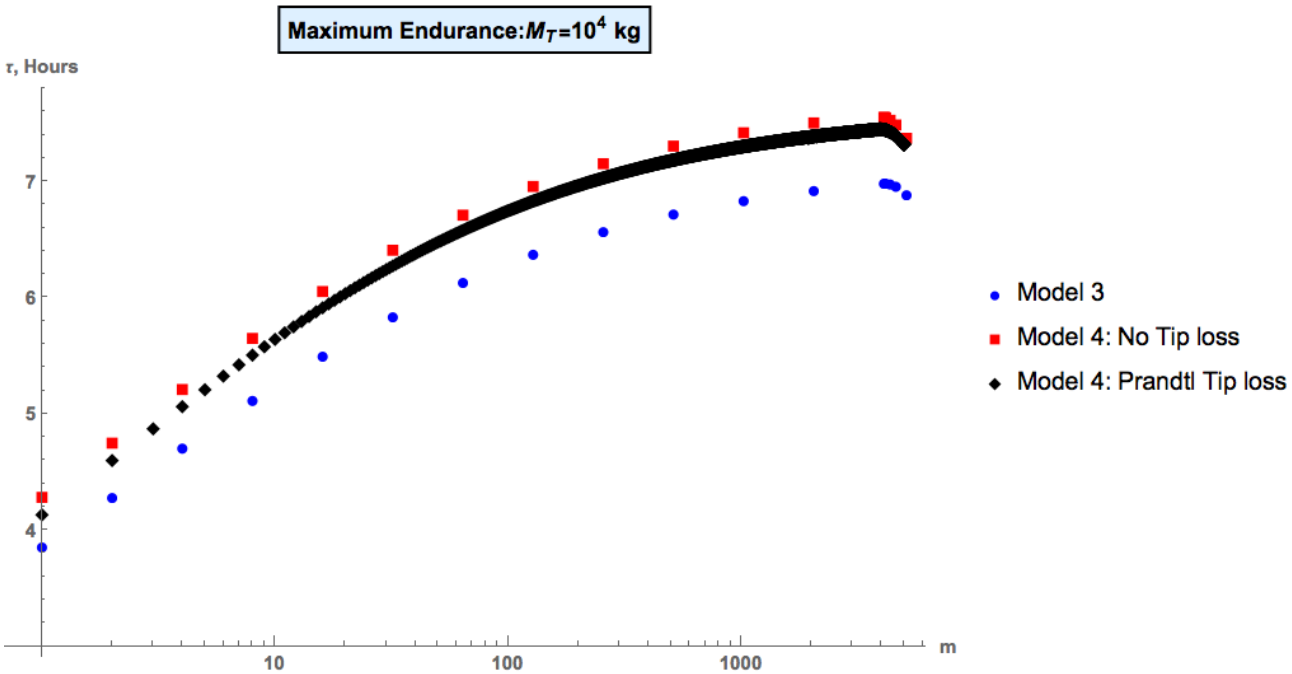

Figure 4.41: Endurance variation with multiplicity from Model 3 and 4 for $M_T = 10^4$kg, b=2, TR=1

Figures 4.42, 4.43, and 4.44 show the variation of optimized endurance with multiplicity and taper ratio for QQ with 10^2, 10^3, and 10^4 kg MTOM, respectively. It is

shown that highly tapered blades offered the highest endurance with a significant decrease in optimized multiplicity. Therefore, higher endurance can be achieved by using tapered blades with a smaller number of rotors.

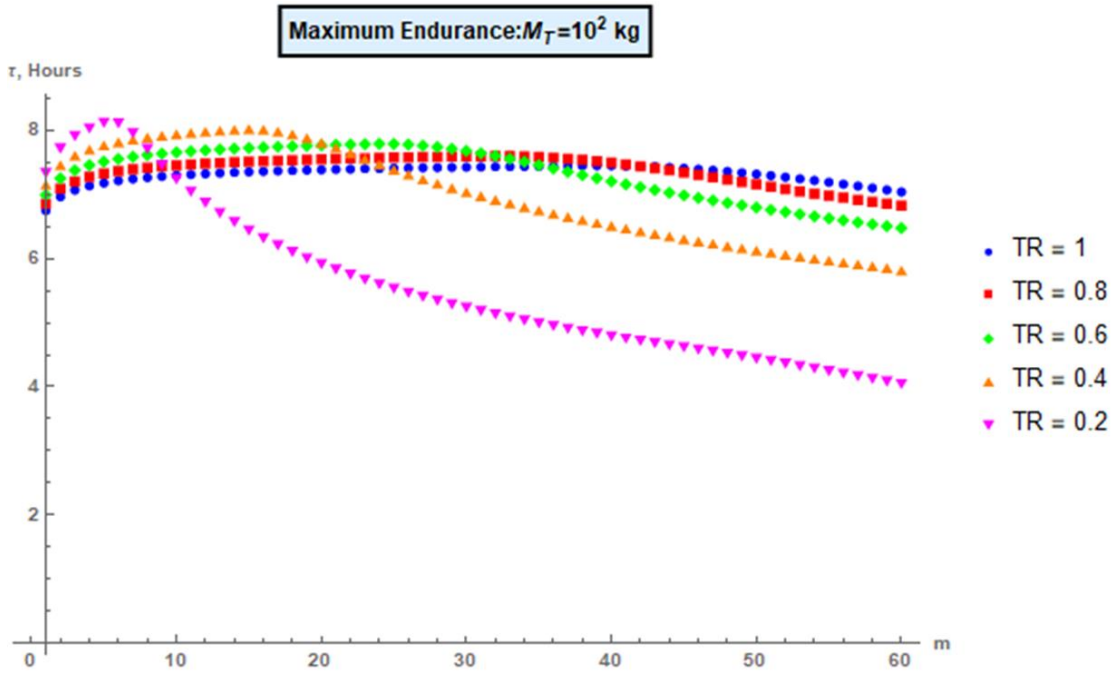

Figure 4.42: Optimized hover endurance from Model 4 with tip losses for $M_T = 10^2$ kg, b=2

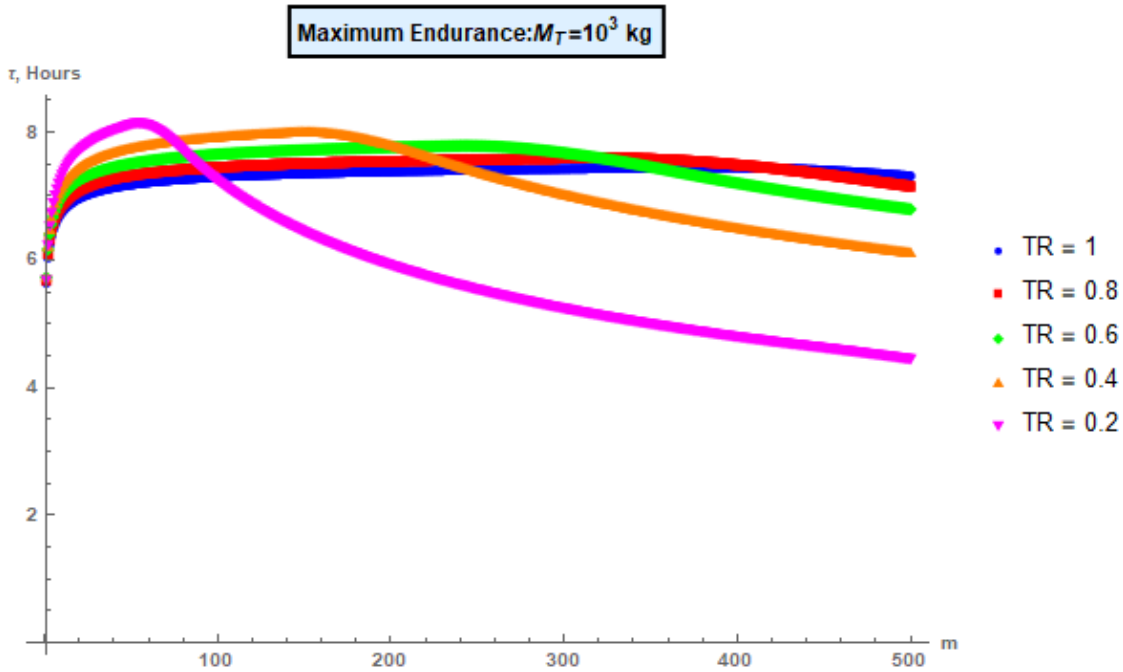

Figure 4.43: Optimized hover endurance from Model 4 with tip losses for $M_T = 10^3$ kg, b=2

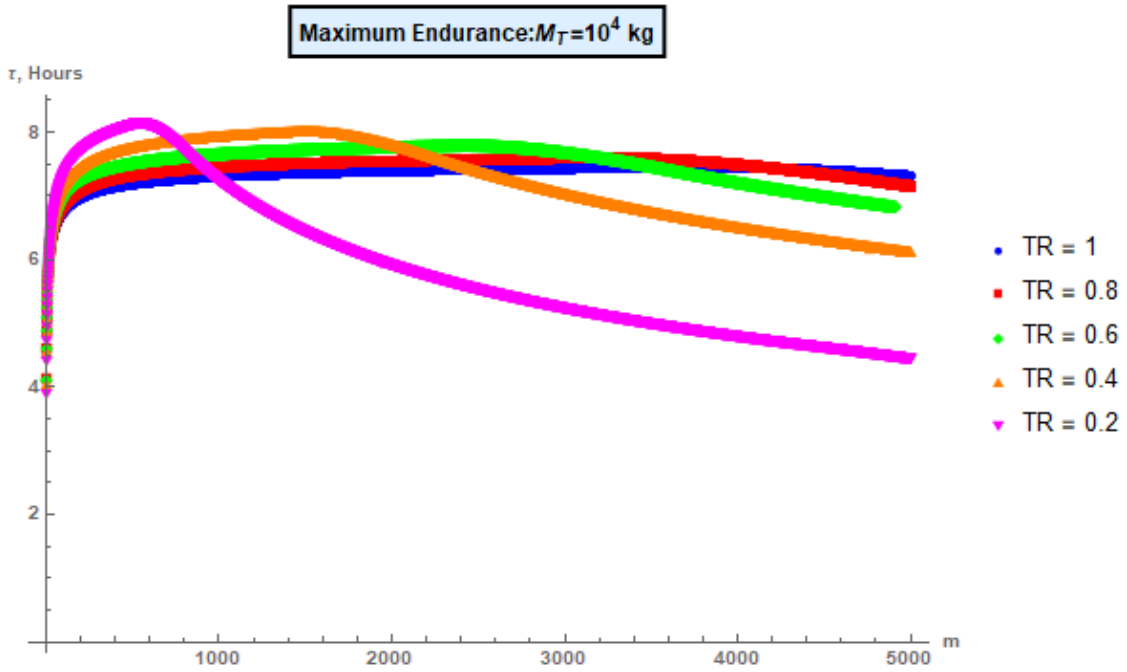

Figure 4.44: Optimized hover endurance from Model 4 with tip losses for $M_T = 10^4$ kg, b=2

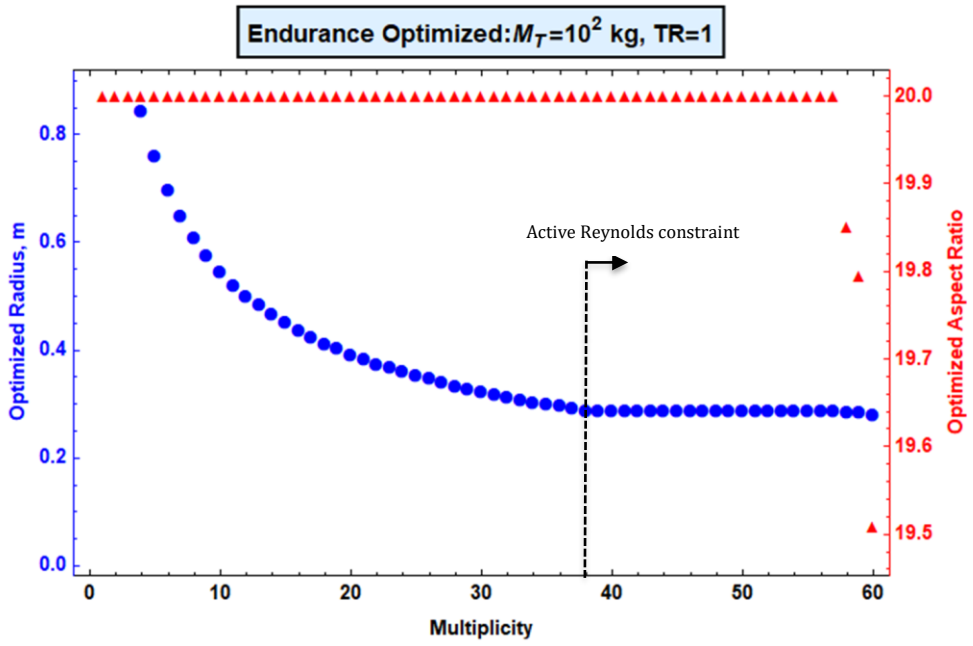

Figure 4.45: Endurance optimized radius and aspect ratio variation for $M_T = 10^2$ kg, TR=1

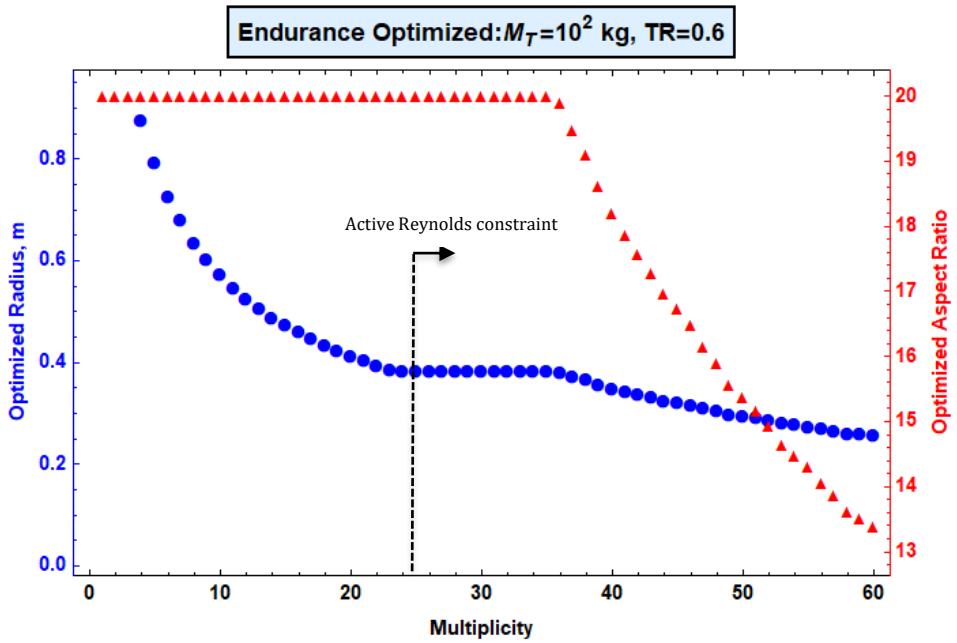

Figure 4.46: Endurance optimized radius and aspect ratio variation for $M_T = 10^2$ kg, TR=0.6

Variation of endurance optimized radius and aspect ratio with multiplicity, for a 100 kg QQ with a taper ratio of 1 and 0.6, is illustrated in Figs. 4.45 and 4.46, respectively. The endurance optimized radius decreases with an increase in multiplicity until the Reynolds number constraint becomes active. Further, an increase in multiplicity results in no change in the optimized radius to a certain point. Thereafter, both the endurance optimized multiplicity and the optimized aspect ratio decreases. This behavior becomes evident for blades with low taper ratios.

Figures 4.47, 4.48, and 4.49 show the variation of Optimized endurance and optimized multiplicity, with taper ratio for a QQ with 10^2, 10^3, and 10^4 kg MTOM, respectively. It is observed that as the taper ratio is decreased, the optimized endurance increases, and the optimized multiplicity decreases. Therefore, using highly tapered blades a QQ providing high endurance can be built with a smaller number of rotors.

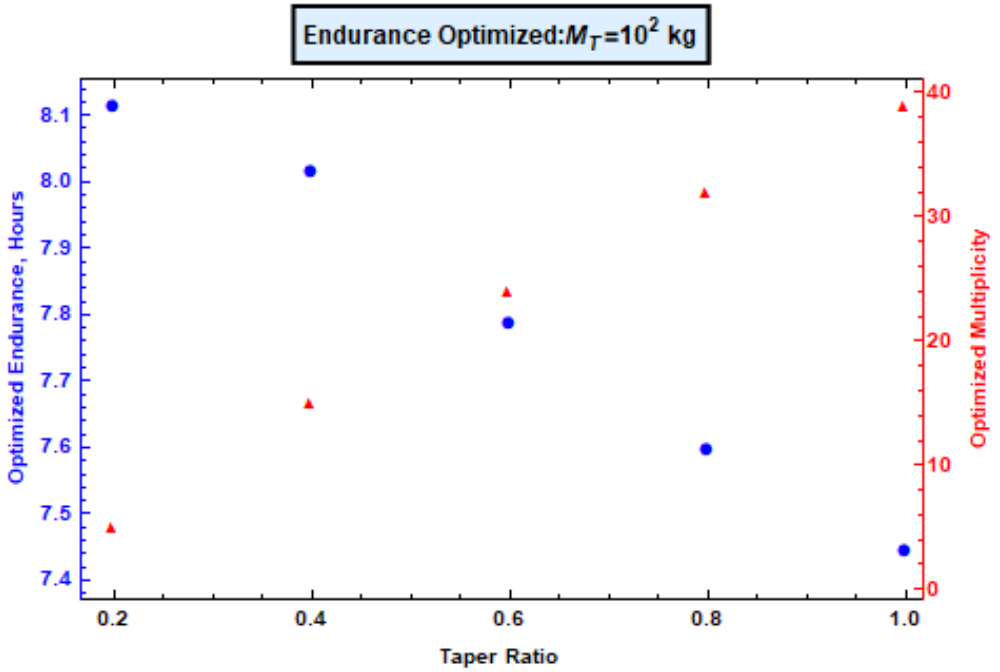

Figure 4.47: Optimized endurance and multiplicity variation with taper ratio for $M_T = 10^2$ kg

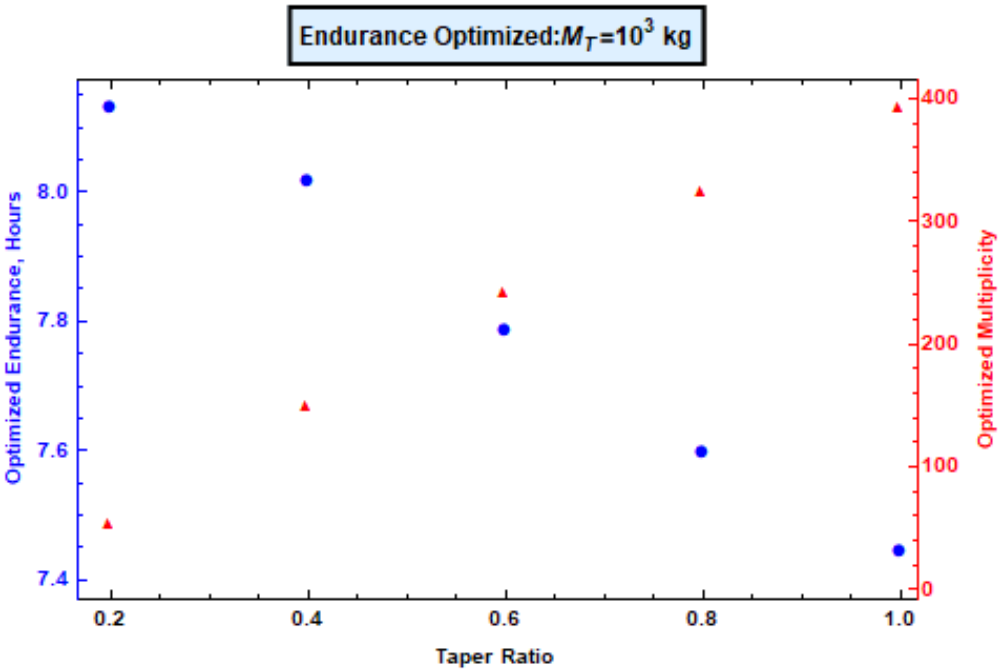

Figure 4.48: Optimized endurance and multiplicity variation with taper ratio for $M_T = 10^3$ kg

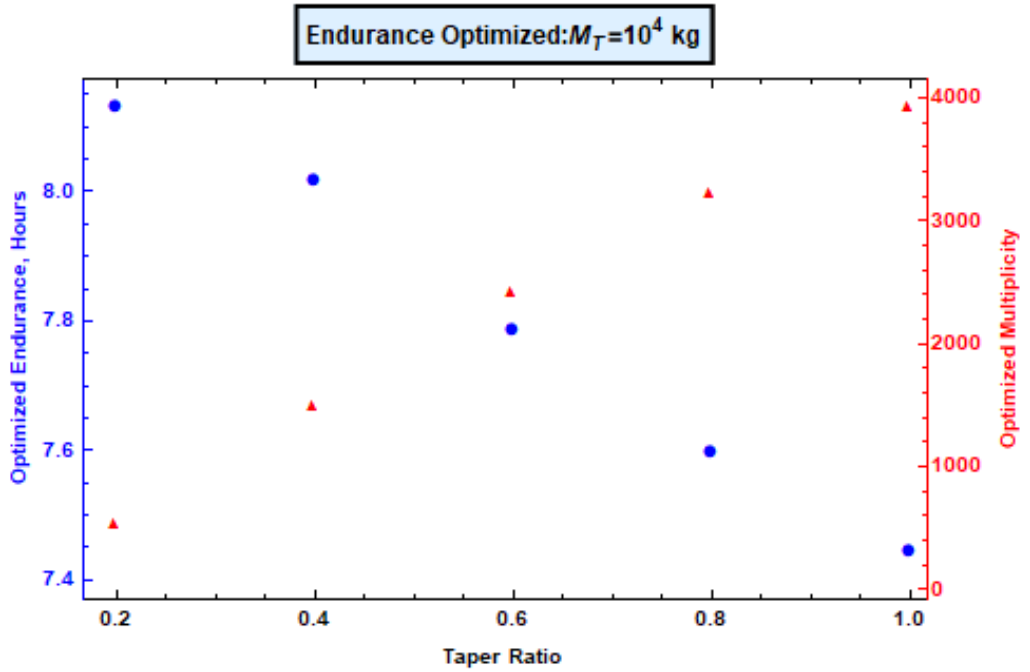

Figure 4.49: Optimized endurance and multiplicity variation with taper ratio for $M_T = 10^4$ kg

Table 4.5 summarizes the optimized endurance values for two-bladed quasi-quadrotors using Model 4 considering tip losses. At low total mass 10^{-1}kg, the blades with an aspect ratio of 5 provide the highest endurance and in contrast, a total mass greater than 10kg, the rotor blades with an aspect ratio of 20 provide the maximum endurance. However, the maximized endurance achievable at smaller M_T is very low when compared to higher M_T as observed in Model 2 and 3. Moreover, at low total mass 10^{-1} and 10^0 kg, rectangular blades provide the highest endurance and in contrast, at a total mass of 10kg, the rotor blades with a moderate taper ratio provide maximum endurance. Furthermore, highly tapered blades offer maximum endurance for QQ with 10^2, 10^3, and 10^4 kg MTOM. Figure 4.50 shows the endurance optimized total mass breakdown as a percentage of MTOM for all mass scales considered. This shows that electric QQ are at a disadvantage compared to IC-based rotorcraft as their weight does not change during the duration of the flight.

Moreover, we observe for the considered taper ratio that an endurance optimized pod exists (highlighted in the table), allowing any larger vehicle to be

conceived by adding optimized pods in multiples of four, until the total weight desired, with no penalty in endurance.

Table 4.5: Endurance optimized results summary from Model 4 considering tip losses

M_T, kg	m	TR	Λ	R, m	τ, Hours
10^{-1}	1	1	5	0.07153	2.81309
10^{0}	1	1	13.054	0.18674	6.16588
10^{1}	1	0.4	20	0.59261	7.93834
10^{2}	5	0.2	20	0.85855	8.11530
10^{3}	54	0.2	20	0.85855	8.11530
10^{4}	543	0.2	20	0.85855	8.11530

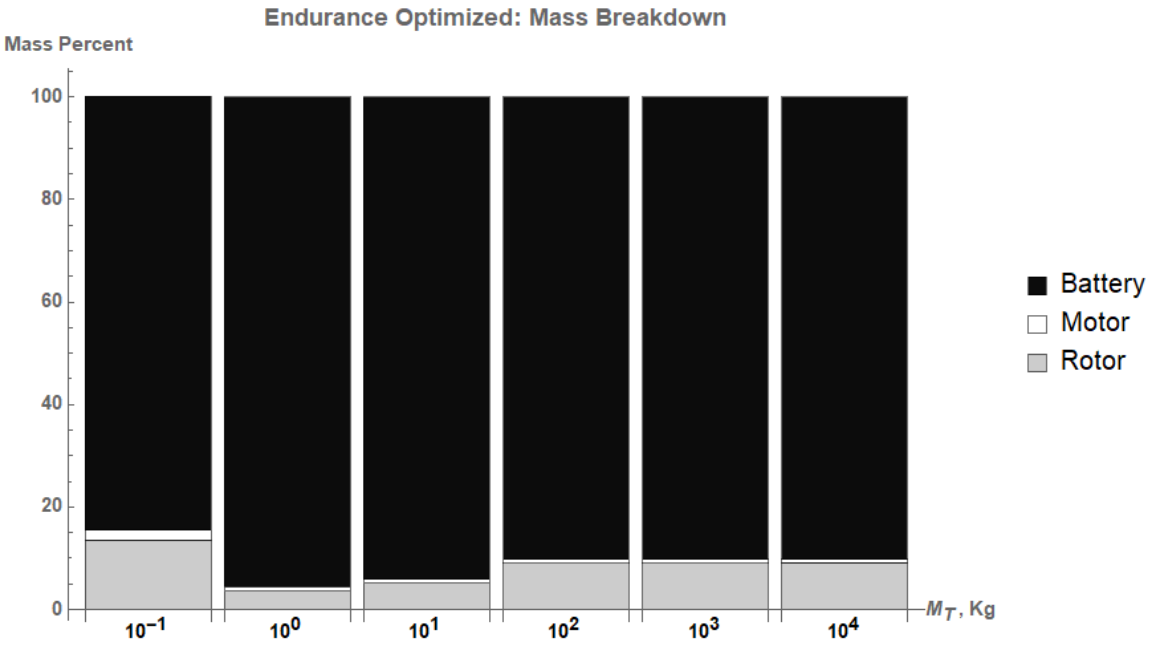

Figure 4.50: Endurance optimized total mass breakdown as a percentage of MTOM

4.4 Sensitivity Analysis

Sensitivity analysis allows us to further understand the influence of the parameters considered on the maximum endurance of the QQ and its optimum configuration. Therefore, considering the propulsor pod powered by Li-Ion batteries, driven by an electric motor with a specific power of 6 kW/kg, and operating at standard sea-level conditions as a baseline, the study was repeated by varying only one parameter. The three parameters considered are

1. Specific energy of the battery
2. Specific power of the electric motor, and
3. Optimization at the hot and high condition

4.4.1 Specific Energy of Battery

Li-S battery chemistry with a theoretical specific energy of 2570 Wh/kg was considered to power the electric motor instead of Li-Ion batteries and the study was repeated using Model 4 considering tip losses. Although Li-S batteries have low specific power when compared to Li-Ion batteries, Li-S batteries could be used as the power demands of optimized low disk loading propulsor pods are less.

It is observed that due to the high theoretical specific energy of Li-S batteries, there is a significant increase in the optimized endurance. Although the optimized endurance was increased by a factor of 6.6 in all cases, it is found that the optimum pod size did not vary significantly, and the optimized multiplicity remained the same as the baseline case. Table 4.6 summaries the endurance optimized results for all MTOM considered.

Figures 4.51, 4.52 and 4.53 illustrates the variation of optimized endurance and optimized multiplicity with taper ratio, for QQ with 10^2, 10^3 and 10^4 kg MTOM, respectively.

Table 4.6: Endurance optimized results summary using Li-S battery chemistry

M_T, kg	m	TR	Λ	R, m	τ, Hours
10^{-1}	1	1	5	0.07153	18.5376
10^{0}	1	1	13.178	0.18852	40.6352
10^{1}	1	0.4	20	0.59260	52.3116
10^{2}	5	0.2	20	0.85832	53.5987
10^{3}	54	0.2	20	0.85832	53.5987
10^{4}	543	0.2	20	0.85832	53.5987

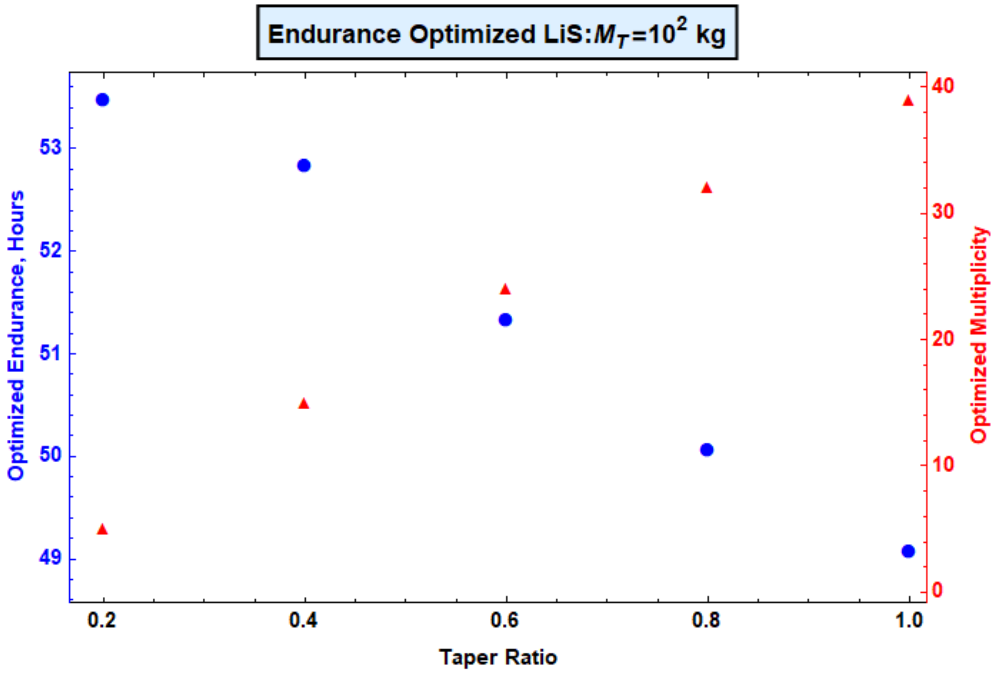

Figure 4.51: Optimized endurance and multiplicity variation using Li-S batteries for $M_T = 10^2$ kg

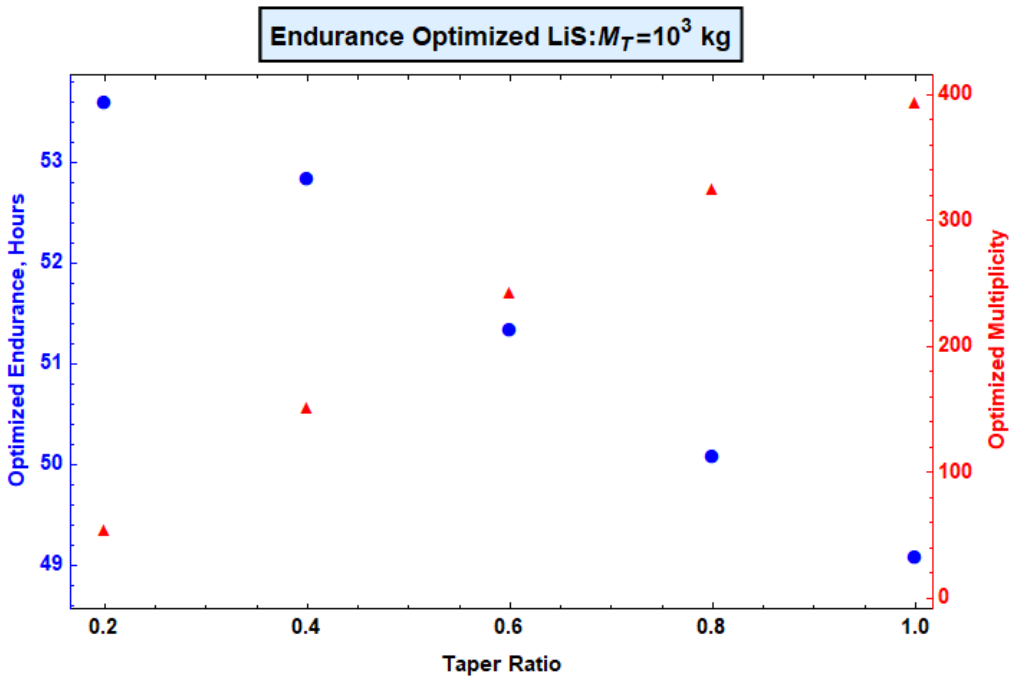

Figure 4.52: Optimized endurance and multiplicity variation using Li-S batteries for $M_T = 10^3$ kg

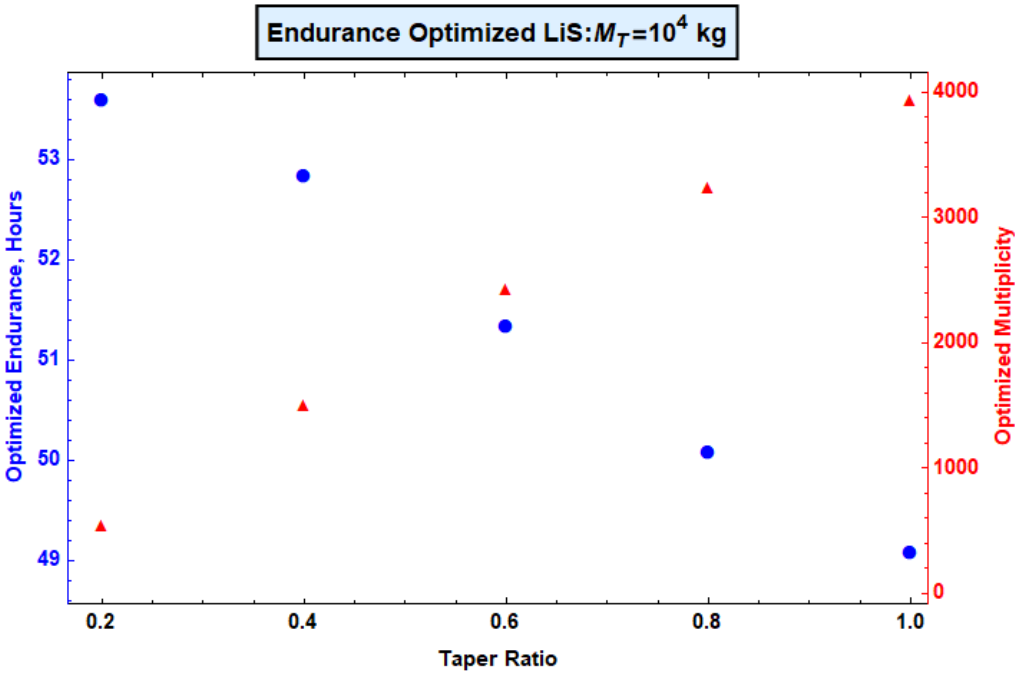

Figure 4.53: Optimized endurance and multiplicity variation using Li-S batteries for $M_T = 10^4$ kg

4.4.2 Specific Power of Electric Motor

A conservative increase of 15% of the specific power of electric motor could be expected in the near future due to the high demands of eVTOL vehicles and electric cars. Therefore, a specific power of 6.9 kW/kg was considered, and the study was repeated using Model 4 including tip losses to estimate power required to hover.

Unlike the previous case, there was only a small increase in the optimized endurance value when compared to baseline, as the optimized propulsor pod weight is mostly battery weight. Table 4.7 summaries the endurance optimized results for all MTOM considered.

Figures 4.54, 4.55, and 4.56 illustrate the variation of optimized endurance and optimized multiplicity with taper ratio, for QQ with 10^2, 10^3, and 10^4 kg MTOM, respectively.

Table 4.7: Endurance optimized results summary with β=6.9 kW/kg

M_T, kg	m	TR	Λ	R, m	τ, Hours
10^{-1}	1	1	5	0.07153	2.82157
10^0	1	1	13.178	0.18852	6.17490
10^1	1	0.4	20	0.59261	7.94682
10^2	5	0.2	20	0.85832	8.14212
10^3	54	0.2	20	0.85832	8.14212
10^4	543	0.2	20	0.85832	8.14212

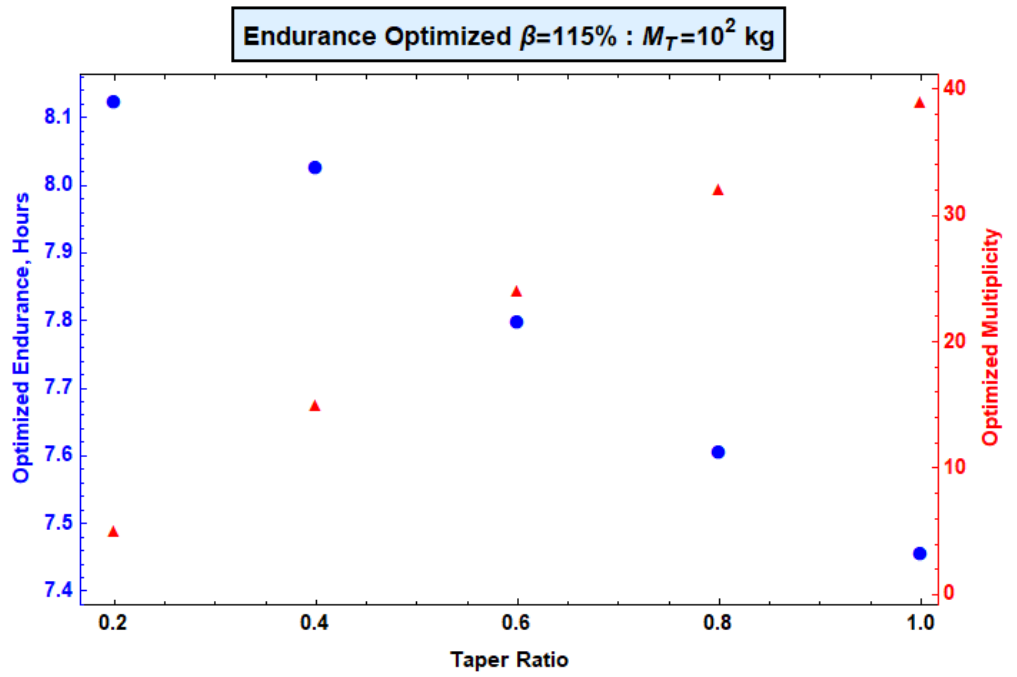

Figure 4.54: Optimized endurance and multiplicity variation for $M_T = 10^2$ kg, β=6.9kW/kg

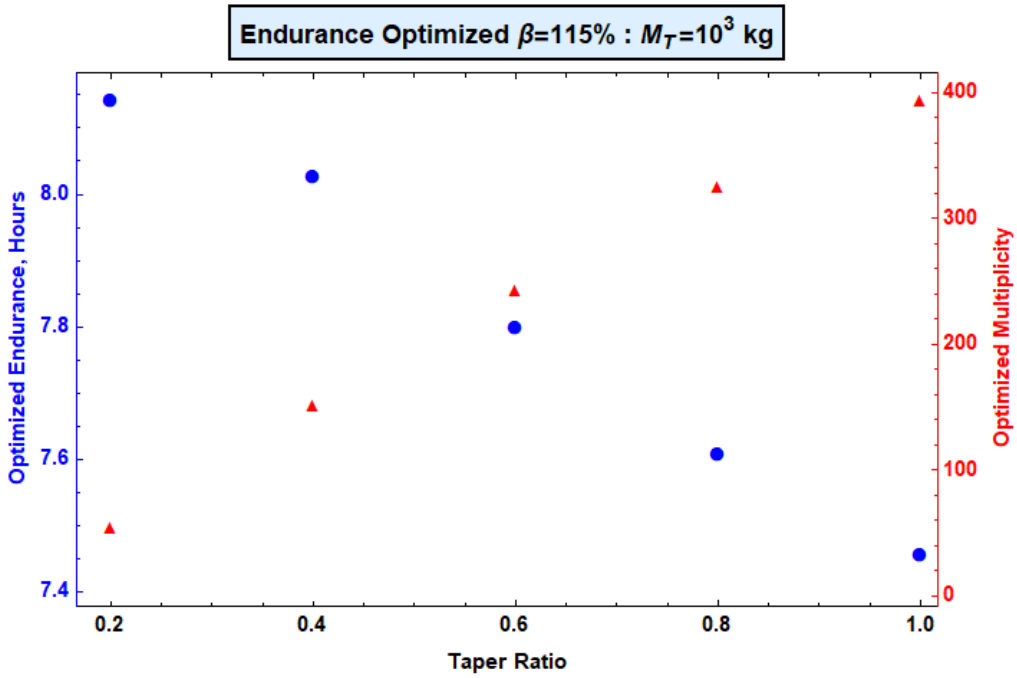

Figure 4.55: Optimized endurance and multiplicity variation for $M_T = 10^3$kg, β=6.9kW/kg

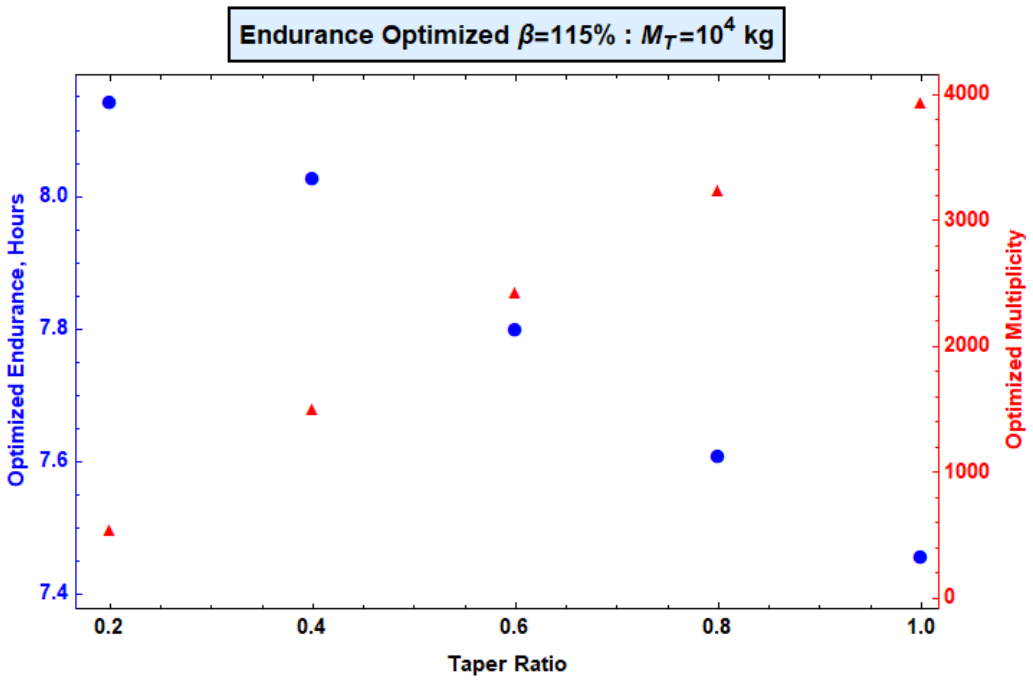

Figure 4.56: Optimized endurance and multiplicity variation for $M_T = 10^4$kg, β=6.9kW/kg

4.4.2 Optimization at Hot and High Condition

Rotorcraft, especially which serves the military are required to operate at very high altitudes when the ambient temperature is high. This operating condition is generally referred to as hot and high conditions. For the United States army, the current design requirements are to efficiently operate at a pressure altitude of 4000 ft with an ambient temperature of 95 F.

Both the increase in altitude and the increase in ambient temperature results in a decrease in air density. In the case of rotorcraft powered by IC engines, the decrease in air density leads to adverse effects on engine performance and the aerodynamic forces generated by the rotor. Unlike IC combustion engines, electric motors do not depend on ambient air to produce power. However, the cooling needs of electric motors may increase, as the ambient temperature is higher compared to sea level. For the present study, the cooling needs of the motor were neglected as a rubber motor model was considered.

As the Federal aviation administration under part 107, restricts the operation of unmanned aerial vehicles less than 55 lbs to low altitudes, QQ with 10^2, 10^3, and 10^4 kg MTOM are only considered. The QQ is optimized at a pressure altitude of 4000 ft with an ambient temperature of 95 F, Table 4.7 summaries the endurance optimized results. The optimized propulsor pod differed from the baseline as the Reynolds number constraint is also influenced in addition to the performance of the propulsor.

Figures 4.57, 4.58, and 4.59 illustrate the variation of optimized endurance and optimized multiplicity with taper ratio, for QQ with 10^2, 10^3, and 10^4 kg MTOM, respectively.

Table 4.7: Endurance optimized results summary at hot and high conditions

M_T, kg	m	TR	Λ	R, m	τ, Hours
10^2	6	0.3	20	0.86180	7.25846
10^3	57	0.3	20	0.86180	7.25846
10^4	571	0.3	20	0.86180	7.25846

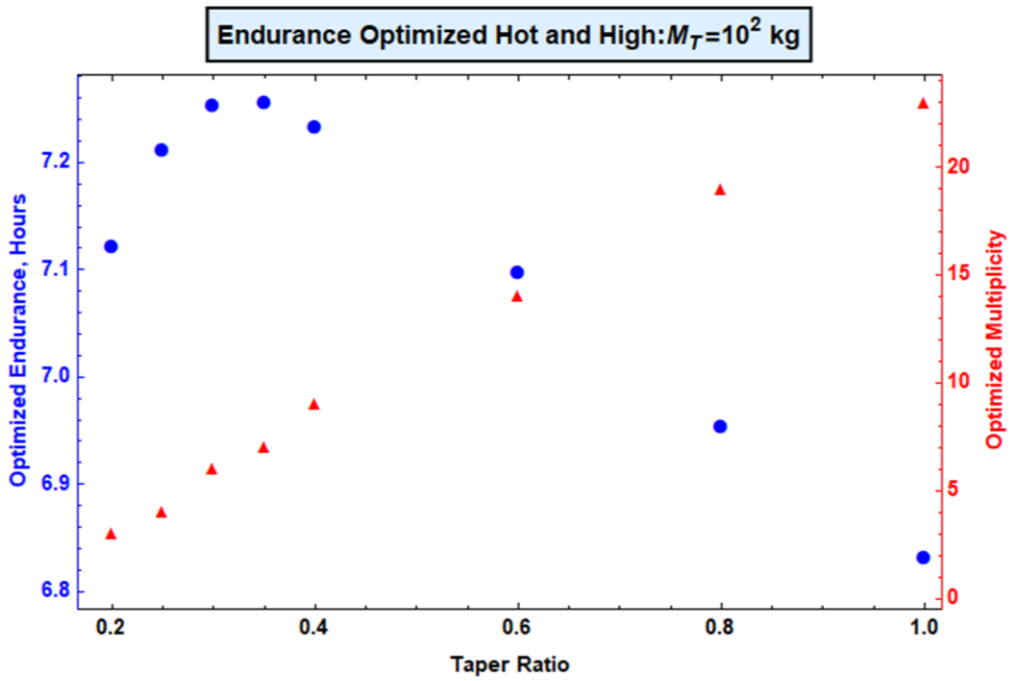

Figure 4.57: Optimized endurance and multiplicity variation for $M_T = 10^2$kg at hot and high condition

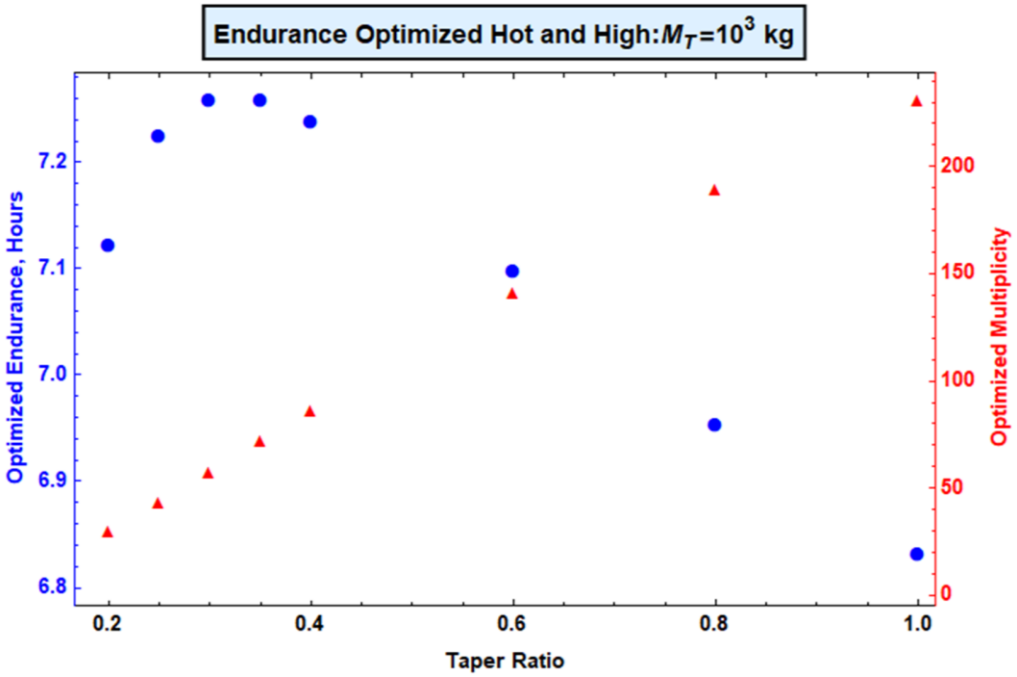

Figure 4.58: Optimized endurance and multiplicity variation for $M_T = 10^3$kg at hot and high condition

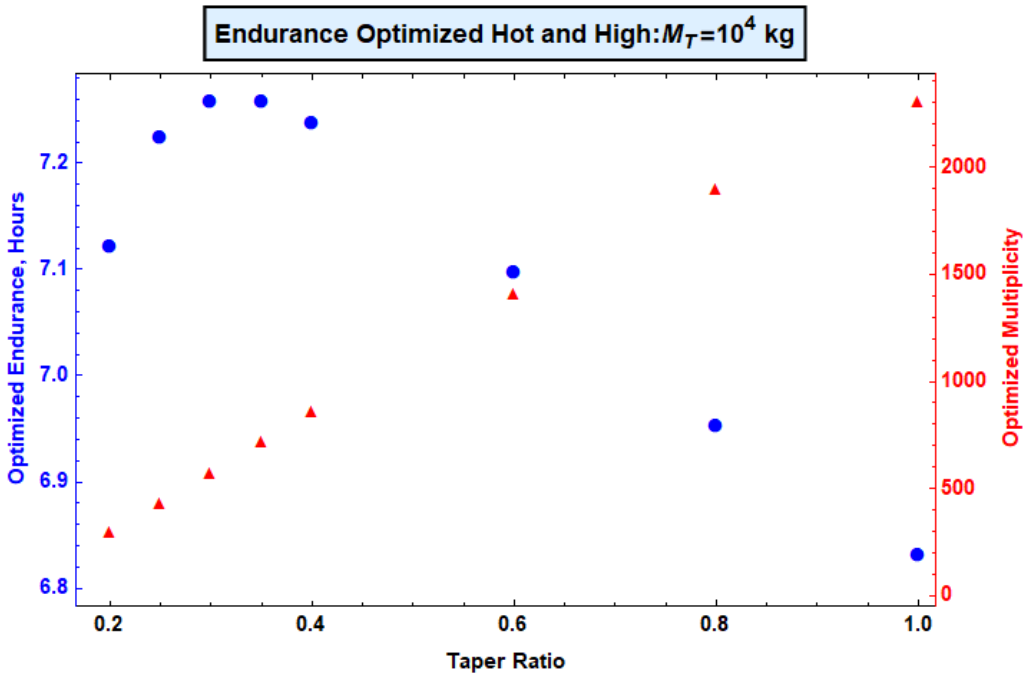

Figure 4.59: Optimized endurance and multiplicity variation for $M_T = 10^4$kg at hot and high condition

5. Conclusions

Using analytical models to estimate hover power required and assuming present-day motor technology with theoretical specific energy for battery, the present study has established the feasible design space using physics-based constraints, has introduced a methodology to estimate the hover endurance for electric QQ VTOL vehicles, and has identified the absolute upper bound of hover endurance achievable by a QQ VTOL configuration across several orders of magnitude, M_T varying from 10^{-1} kg to 10^4 kg.

Additionally, by performing a constrained optimization for two bladed electric QQ VTOL across several orders of magnitude of MTOM and considering the tip speed as constant, it is shown in this study that on the one hand, individual propulsor pods which are too small cannot be optimal in hover, as low Reynolds number has adverse effects on aerodynamics, while on the other hand, pods that are too large cannot be optimal in hover as the blade mass is too high. Consequently, it is found that an optimal propulsor pod exists, for which the hover endurance is optimized. Hence, modular design for QQ VTOL configurations can be achieved for larger vehicles leveraging multiple such optimal pods.

It is inferred from the optimization of QQ at various orders of magnitude, M_T varying from 10^{-1} kg to 10^4 kg, that below a total mass where QQ vehicles cannot leverage high endurance of optimal propulsor pods, the hover endurance decreases with a decrease in the total mass. Suggesting that QQ vehicles with the low MTOM are the most susceptible to adverse effects caused by low Reynolds number.

Furthermore, estimating the power required to hover using multiple models with an increasing refinement not only provided valuable insight into the effects of scaling up vehicle size upon optimal vehicle configuration and optimal vehicle hover endurance, but also aided in ensuring the convergence of gradient-based numerical optimization procedure by providing an initial estimate of the parameters.

Endurance optimized results show that for QQ with 10^{-1} kg and 10^0 kg MTOM, a quadrotor design with low aspect ratio blades provides high endurance, as an

increase in multiplicity or a decrease in taper ratio would further decrease the tip Reynolds number. For QQ with 10 kg MTOM, although there was a slight increase in endurance value with an increase in multiplicity for propulsor pods with rectangular blades, a quadrotor design with moderately tapered blades is found to be optimum.

Moreover, for QQ with 10^2 kg, 10^3 kg, and 10^4 kg MTOM, a modular distributed propulsion configuration with highly tapered blades offered maximum endurance. It is also observed that endurance optimized propulsor pod geometry is the same for QQ with 10^2 kg, 10^3 kg, and 10^4 kg MTOM, and the optimum propulsor pod geometry varies with taper ratio. The endurance optimized propulsor pod solution is determined by an optimum for which the upper limit in blade aspect ratio is active i.e., Λ=20 is an educated choice, absent a blade design considering aeroelasticity and structural demands. Additionally, highly tapered blades offer a significant decrease in endurance optimized multiplicity when compared to propulsor pods with rectangular blades. Therefore, high hover endurance can be achieved using a smaller number of propulsor pods with tapered blades.

For the endurance optimized QQ VTOL with 10^2 kg, 10^3 kg, and 10^4 kg MTOM, the total mass of rotor, motor, and battery are 9.04%, 0.721%, and 90.23% of the MTOM, respectively. The total power required to hover, calculated using blade element momentum theory considering Prandtl's tip loss function for the endurance optimized individual propulsor pod with a disk loading of 19.6230 N/m^2 is 200.323 W. Compared to Siemens electric motor with a continuous power of 260 kW, the optimized propulsor pod requires three orders of magnitude less power. This is possible due to the endurance optimized low disk loading rotors with linearly twisted, highly tapered blades. Hence, modular distributed propulsion electric QQ VTOL configurations achieve higher hover endurance leveraging multiple such low disk loading optimal pods. However, low disk loading propulsors are not optimal in forward flight.

Sensitivity studies show that varying the theoretical specific energy of the battery from 390 Wh/kg for Li-Ion chemistry to 2570 Wh/kg for Li-S chemistry, resulted in a significant increase in optimized hover endurance, by a factor of 6.6, as

the endurance optimized optimal propulsor pod consists of approximately 90% of battery by mass. However, an increase of 15% of the specific power of the electric motor, resulted in a slight increase in optimal hover endurance suggesting that improvements to battery chemistry offer higher endurance values.

From the optimization of QQ VTOL at hot and high conditions, it is found that moderately tapered blades with a taper ratio no less than 0.3 should be used to achieve high endurance values. An increase in altitude results in low air density, and an increase in the ambient temperature results in a decrease in air density and an increase in the viscosity of air, at hot and high conditions Reynolds number decreases. Therefore, moderately tapered blades are optimum as the blade tip Reynolds number further decreases with a decrease in the taper ratio. Moreover, the geometry of the optimized propulsor pod varies with the baseline, due to the change in operating conditions.

6. Recommendations for Future Work

The research effort undertaken has identified that an optimized propulsor pod exits for which the hover endurance is maximum. In this chapter, several aspects that require further attention to improve the hover endurance and to further understand the effects of scaling on hover performance for an electric QQ are identified as recommended topics for future research.

Due to the conceptual nature of the present study and in order to uncouple the scaling of the propulsor pod, rubber models were considered for the mass estimation of the battery and the motor. Inclusion of advanced models accounting for the losses and cooling needs, for the battery and the motor-ESC would further increase the accuracy in the prediction of hover endurance. Moreover, the energy available as a function of the rate of discharge of the battery, and the efficiency dependence of the electric motor on the operating torque and RPM could be included in future studies.

As the endurance optimized results suggest that the optimized propulsor pod contains approximately 90% of battery by mass, a different source for energy such as fuel cells or hybrid electric could be considered. This would allow the total mass of the vehicle to decrease over the duration of operation thereby increasing endurance.

In the present study, the mass estimation of the rotor was based solely on the geometry of the solid propulsor blade. The propulsor blade itself could be optimized to decrease its mass considering the structural demands and aeroelasticity. Consequently, propulsors with larger aspect ratio blades and potentially resulting in lower blade loading could result which would further increase endurance by decreasing the induced power required. Such an improved model would also allow an understanding of the effects of higher number of blades on the scaling of QQ.

An aero-structural optimization considering the variation of the airfoil and the platform along the span would result in efficiently identifying the optimum propulsor pod geometry. In the present study, the operating conditions were limited to blade tip Reynolds number to be greater than 10^5 however, the constraints could be relaxed

to Reynolds number over the span of the blade where the thrust gradients are higher to be greater than 10^5.

Rotor-Rotor interactions were disregarded in the present study to estimate the upper bound of hover endurance achievable. These viscous interactions can be included in the total power calculations using advanced methods such as computational aerodynamics or viscous vortex particle methods. Although these models increase the accuracy of power required to hover, the computational time required is very high.

Another aspect to be included in the scaling investigation is that of the support structure. As the distance of separation between the rotors would on the one hand, influence the power required and while on the other hand, would also define the length/size of the support structure, the scaling is therefore coupled.

Considering mission scenarios such as taking off with a certain payload of know mass and delivering it to one or more locations instead of only hover would also help in understanding mission specific optimized QQ configurations and performance.

Although the gradient-based optimization technique SQP used in this study is efficient, the solution obtained may depend on the initial values of the parameters. The present study leverages the advantage of using multiple models with increasing refinement to estimate the endurance, by providing the results obtained from models with a low refinement as initial conditions to models with high refinement to ensure the convergence of optimization procedure to the global optimum. When estimates of initial conditions are not available, a hybrid optimization scheme consisting of a non-gradient-based algorithm to initially identify the region of global maximum followed by a gradient-based algorithm to refine the solution could be used to ensure the convergence of optimization procedure to the global optimum.

References

[1]Stepniewski, W. Z., and Shim, R. A.., "A Comparative Study of Soviet vs. Western Helicopters Part 2 - Evaluation of Weight, Maintainability, and Design Aspects of Major Components", NASA Contractor Report 3580, 1983.

[2]Hepperle, M., "Electric Flight – Potential and Limitations," NATO Report STO-MP-AVT-209.

[3]Nagaraj, V. T and Chopra, I., "Explorations of Novel Powerplant Architectures for Hybrid Electric Helicopters", AHS Annual Forum Proceedings, Montreal, Canada, May 2014.

[4]Bouabdallah, S., and Siegwart, R., "Design and Control of a Miniature Quadrotor," Advances in Unmanned Aerial Vehicles, Springer Netherlands, 2007.

[5]Gur, O., and Rosen, A., "Optimizing Electric Propulsion Systems for UAVs," AIAA 2008-5916. 12th AIAA/ISSMO Multidisciplinary Analysis and Optimization Conference, Victoria, British Columbia, Canada, September 2008.

[6]Lundstroom, D., Amadori, K., and Krus, P., "Automation of Design and Prototyping of Micro Aerial Vehicle", AIAA-2009-629, 47th AIAA Aerospace Sciences Meeting, Orlando, FL, USA, January 2009.

[7]Bohorquez, F., Pines, D., and Samuel, P.D., "Small Rotor Design Optimization Using Blade Element Momentum Theory and Hover Tests", Journal of Aircraft, 2010.

[8]Harrington, A. M., "Optimal Propulsion System Design for a Micro Quad Rotor", Master's Thesis, Department of Aerospace Engineering, University of Maryland, College Park, 2011.

[9]Latorre, A. M., "Propulsion system optimization for an unmanned lightweight quadrotor," M.S. Thesis, Department of Aerospace Engineering, Universität Politecnica de Catalunya, Catalonia, Spain, 2011.

[10]Ampatis, C., and Papadopoulos, E. "Parametric Design and Optimization of Multi-Rotor Aerial Vehicles." In Applications of Mathematics and Informatics in Science and Engineering, pp. 1-25. Springer International Publishing, 2014.

[11]Beals, N., "Design of Small Rotor for Multicopter UAS", AHS Forum 73, May 2017.

[12]Choi, T. P., Soban, D. S and Mavris, D, N., "Creation of a Design Framework for All-Electric Aircraft Propulsion Architectures", 3rd International Energy Conversion Engineering Conference, San Francisco, California, August 2005.

[13]Sinsay, J. D., Alonso, J. J., Kontinos, D., Melton, J, E and Grabbe, S., "Air Vehicle Design and Technology Considerations for an Electric VTOL Metro-Regional Public Transportation System", AIAA Aviation Technology, Integration, operations Conference, Indianapolis, Indiana, September 2012.

[14]Patterson, M. D., German, B. J., and Moore, M. D., Performance Analysis and Design of On-Demand Electric Aircraft concepts," 12th AIAA Aviation Technology, Integration, and Operations (ATIO) Conference, Indianapolis, Indiana, September 2012.

[15]Moore, M. D., "Concept of Operations for Highly Autonomous Electric Zip Aviation," 12th AIAA Aviation Technology, Integration, and Operations (ATIO) Conference, Indianapolis, Indiana, September 2012.

[16]Datta, A and Johnson, W., "Powerplant Design and Performance Analysis of a Manned All-Electric Helicopter", Journal of Propulsion and Power, Vol. 30, No. 2, April 2014.

[17]Pokhrel, M., Gladin, J. C., Ali, K., Collins, K. and Mavris, D. N.," Modeling and Requirements Definition for a Hybrid-Electric Powered Helicopter", AHS Sustainability Conference, Montreal, Quebec, Canada, September 2015.

[18]Snyder, C, A.," Personal Rotorcraft Design and Performance with Electric Hybridization", AHS 73rd Annual Forum, Fort Worth, TX, May 2017.

[19]Johnson W., and Silva C., "Concept Vehicles for VTOL Air Taxi Operations," AHS Technical Conference on Aeromechanics Design for Transformative Vertical Flight, San Francisco, CA, January 2018.

[20]Silva, C., Johnson, W., Antcliff, K., and Patterson, M., "VTOL Urban Air Mobility Concept Vehicles for Technology Development," AIAA Aviation Forum, Atlanta, GA, 2018.

[21]Wanyi N., and Datta, A., "Development of Models for Electrochemical Power and Sizing of Electric-VTOL Aircraft," AIAA SciTech Forum, Kissimmee, Florida, January 2018.

[22]Venepalli B., and Dancila D. S., "Scaling Investigation of Electric Quasi-Quadrotor Hover Endurance," VFS Autonomous VTOL Technical Meeting and Electric VTOL Symposium, Mesa, Arizona, January 2019.

[23]Duffy, M., and Samaritano, T., "The LIFT! Project – Modular, Electric Vertical Lift System," Proceedings of the 71st AHS Annual Forum, Virginia Beach, VA, May 2015.

[24]Duffy M., and Samaritano T., "The LIFT! Project – Modular, Electric Vertical Lift System with Ground Power Tether," 33rd AIAA Applied Aerodynamics Conference, Dallas, TX, June 2015.

[25]Winslow, J., Benedict, M., Hrishikeshavan, V., and Chopra, I., "Design development and flight testing of a high endurance micro quadrotor," *International Journal of Micro Air Vehicles*, Vol. 8 (2016), pp.155-169.

[26]Gatti, M., Giulietti, F., and Turci, M., "Maximum endurance for battery-powered rotary-wing aircraft," *Journal of Aerospace Science and Technology*, Vol. 45 (2015), pp. 174-179.

[27]Traub L. W., "Range and endurance estimates for battery-powered aircraft," *Journal of Aircraft*, Vol. 48, No. 2 (2011), pp. 703-707.

[28]Winslow, J., Otsuka, H., Govindarajan, G., and Chopra, I., "Basic Understanding of Airfoil Characteristics at Low Reynolds Numbers (10^4–10^5)," *Journal of Aircraft*, Vol. 55, No. 3 (2018), pp. 1050-1061.

[29]Govindarajan, M., Sridharan, A., and Chopra, I., "A Scalability Study of the Multirotor Biplane Tailsitter using Conceptual Sizing," Proceedings of the 74th American Helicopter Society Annual Forum, Phoenix, AZ, May 14–17, 2018.

[30]Govindarajan, M., Sridharan, A., and Avera, M., "Integration of Physics Based Weight Models into Rotorcraft Design Sizing," Proceedings of the 43rd European

Rotorcraft Forum, Milan, Italy, Sep 12–15, 2017.

[31]"Kokam Batteries, accessed July 18th, 2020," http://kokam.com/cell/.

[32]"Siemens Electric Flight, accessed July 18th, 2020,"

www.siemens.com/press/electric-aircraft .

[33]Walter, C, S., "Design of High-Torque-Density Synchronous Drives for Propulsion of Rotary-Wing Aircraft," Ph.D. Thesis, TU Delft, 2016.

[34]Crabtree, J, A., "Weight Estimation for Helicopter Design Analysis," Society of Allies Weight Engineers, 17th Annual Conference, Belmont Plaza Hotel, New York, New York, May 1958.

[35]Prouty, R, W., *Helicopter Performance Stability and Control*, Krieger, Malabar, FL, 1995, p. 663.

[36]Leishman, J, G., *Principles of Helicopter Aerodynamics*, Cambridge University Press, New York, NY, 2000.

[37]Johnson, W., *Rotorcraft Aeromechanics*, Cambridge University Press, New York, NY, 2013.

[38]Dreier, M., *Introduction to Helicopter and Tiltrotor Flight Simulation*, American Institute of Aeronautics and Astronautics, Inc., Reston, VA, 2018, p. 614.

[39]Vanderplaats, G., *Multidiscipline Design Optimization*, Vanderplaats Research & Development, Inc., Monterey, CA, 2007, p. 235.

[40]Mathworks® (2020). *Global Optimization Toolbox: Documentation* (r2020a), accessed July 18th, 2020, https://www.mathworks.com/help/index.html?s_tid=CRUX_lftnav.

[41]Castles, W., and Gray, R., "Empirical Relation Between Induced Velocity, Thrust, and Rate of Descent of a Helicopter Rotor as Determined by Wind-Tunnel Tests on Four Model Rotors", NACA Technical Note 2474, 1951.